Master Thesis

Utrecht University

Royal Netherlands Meteorological Institute

Lightning detection with infrasound

Author:
Nicolai Proksch

Supervisors:
Dr. Aarnout van Delden (IMAU)
Dr. Willem-Jan van de Berg (IMAU)
Dr. Jelle Assink (KNMI / RDSA)
Dr. Hidde Leijnse (KNMI /RDWD)

28 January 2017

Royal Netherlands
Meteorological Institute
Ministry of Infrastructure and the Environment

University of Utrecht

Abstract

In this thesis we have looked to validate the different lighting detection systems. Although there have been different lighting detection systems in the Netherlands, it remains difficult to exactly locate and characterize the lighting discharge.
Previous studies have shown that infrasound is sensitive for lighting detection. Infrasound is a soundwave with a low frequency, < 20 Hz, and travels further through the atmosphere than audible soundwaves, 20 – 20,000 Hz. Differently from the electromagnetical (EM) system, the infrasound array is not only tuned to detect lightning. The array picks up a lot of signals which are not lightning signals, so characterization of the soundwave is very important.
In order to validate the different lighting detection sytems we used two different EM detection systems: FLITS and KLDN. FLITS is the previously used sensor of the Royal Netherlands Meteorological Institute (KNMI). KLDN is the current operational system.
In this thesis both of these systems are compared with the infrasound system in order to conclude which of these two sensors is better. The data is compared for a specific thunderstorm that passed at 27/07/2013 9:45 UTC De Bilt. The influence of the atmosphere on wave propagation is examine using data from Numerical Weather Prediction (NWP) model, HARMONIE.
The wind has the largest effect on the propagation. In this study we found that a wave travels further when it goes along the wind. The wave paths are wind dependent.
With the information of propagation and detection we could compare the infrasound detections with the FLITS/KLDN detections, this will be done for cloud-ground discharges (CG).
In conclusion, the wind is a main driver to understand wave propagation. In this case the infrasound system has 15 of the 80 CG discharges from KLDN detected. For FLITS the infrasound system has 5 of the 24 CG discharges detected. If infrasound does not have the signal, this does not mean that there is a miss match. Only the discharges which are detected by the infrasound could be validated.

Contents

1 Introduction

The rumble of thunder is well-known by everybody. It is alerting us that something dangerous is coming. Thunder has an enormous impact on our society: one or two people died due to lightning in The Netherlands every year; material damage of a lightning strike costs the community millions of euros [1]; due to thunder airports ground operations are often obligated to shut down [2]. This costs the airline industry millions of euros. This makes research about thunder still very important.

The Royal Netherlands Meteorological Institute (KNMI) is one of the institutions that take a lead in researching lightning detection. At KNMI there are two different detection systems for lightning discharges; FLITS and KLDN [3]. Those systems work with electromagnetic (EM) radiation. FLITS was the operational lightning detection sensor of the KNMI. Since 2015 KLDN is the current one. However, both of these systems have flaws as they are currently unable to detect lighting discharges at the same time and location. Earlier researches show that infrasound is receptive for lightning discharges [4][5][6]. Infrasound can be a suitable and independent mechanism to validate the lightning detection systems.

1.1 Creation of lighting

A lightning strike is an electrical discharge between two clouds, a cloud to cloud discharge (CC), or between the cloud and the ground (CG). In order for lighting strike to happen we need separation of charge in a cloud. The process behind the charge separation is still not 100% clear.
One key process of the charge separation is the collision between graupel and ice particles. Graupel is precipitation that forms when supercooled water droplets freeze on snowflakes. The collision ensures that the ice particles become positive charged. The graupel becomes negative charged. Due to the fact that graupel is heavy, it will drop to the bottom of the cloud. Ice particles are lighter and therefore go with the updraft to the top of the cloud. Now there is a separation of charge in the cloud. At the top there is positive charge and at the bottom there is negative charge. Now there is a negative charge at the bottom of the cloud and a positive charge at the surface, with the same amount of charge. If the electrical field is strong enough there will be a precursor, with negative ions, from the cloudbase in the direction of the ground. In the opposite way, there will be a precursor, with positive ions, from the ground (mostly from sharp objects) in the direction of the cloud. When those two precursors meet, the main discharge will go through this channel; the lightning strike. The precursor is much weaker than the main discharge. In short a strong electric field combined with charge separation in the cloud can lead to a lightning discharge.
A lightning discharge exists of one or more discharges. The total discharge has a duration in the order of 0.2 seconds. The total discharge is called a flash. The several components of the discharge are strokes. The strokes can only last for less than 0.001 seconds [7].

1.2 What is infrasound?

An infrasound wave is a sound wave. Sound waves are longitudinal waves. The motion of the particle moves the same direction as the propagation. The sound wave is a pressure

wave which velocity is dependent on temperature. When a sound wave moves through the atmosphere, the wave disturbs the equilibrium state of the atmosphere by compressions. Sound waves are elastic, this means that when a particle is displaced, a force proportional to the displacement acts on the air particle to restore it to his original position[8].

If the frequency become higher than 20,000 Hz it is inaudible for humans, this is called ultrasonic sound. On the other side of the spectrum, at a frequency lower than 20 Hz, there is the infrasound. This sound is also inaudible for humans. In the atmosphere there is a limit for the frequency of sound waves. The infrasound frequency is bounded by the thickness of the atmospheric layer. An infrasound wave has an amplitude of hundredths to tens of Pa [9]. An other important attribute of infrasound is that it can travel over long distances through the atmosphere. This is due to its low-frequency content [9].

The pressure fluctuations of the infrasound waves are small in comparison the ambient air pressure. These small fluctuations in pressure are measured by a microbarometer. In section 2.1 there is a more described description about this sensor.

1.3 The source of the infrasound

To generate infrasound, large volumes of air have to shift or surfaces have to move [9]. We identify the different infrasound sources by looking at the characteristics of the signal. This characterisation is frequency versus time signature, duration and direction. Table 1 shows a variety in infrasound sources. These sources are generated by nature, but are also man-made. Examples with data can be found in *Campus* (2004) [10]. There are still infrasound sources that have to be identified, so the list is not comprehensive [10].
Severe convective storms generate infrasound with frequencies between 0.02 and 0.1 Hz. The amplitudes of these waves are 0.5. Other meteorological sources of infrasound are microbursts, lightning, sprites and tornadoes [11]

When lightning strikes it generates infrasound. These are usually short lived disturbances. The frequency range of this infrasound is between 0.5 and 20 Hz and has an amplitude of 0.01 up to 2 Pa [12][13][5]. The dominant frequency of infrasound is 1 Hz. The waves are pulse-like and often travels horizontally. Infrasound from CC lightning however, travels vertically downwards [12].

1.4 Infrasound compared to electromagnetic radiation

The systems KLDN and FLITS use electromagnetic radiation (EM). However, in this study we combine this with infrasound signals. Infrasound and EM radiation work very different. EM radiation travels near the speed of light, $3{\cdot}10^8$ m s^{-1}. Infrasound travels with the speed of sound, around 340 m s^{-1}. This is a factor 10^6 smaller than the propagation speed of EM radiation.

There is a difference between infrasound and EM radiation in measuring the back azimuth. The back azimuth is the angle between sensor and discharge. The angle is measured in respect to the sensor. Due to the wind there is a difference in the observed back azimuth

Infrasound source	**Frequency range (Hz)**	**Maximum observed amplitude (Pa)**	**Estimated maximum detection range (km)**
Atmospheric nuclear explosions	0.002 - 20	>20	>20,000
Bridges and other structures	0.5 - 20	0.5	<100
Aeroplanes	0.3 - 20	2 (sub), 10 (super)	<100 (sub), 5,000 (super)
Volcanic eruptions	0.002 - 20	>20	>20,000
Convective storms	0.02 - 0.1	0.5	>1,500
Tornadoes	0.5-20	0.5	300
Lightning	0.5-20	1.0	50

Table 1: Characteristics of some infrasound sources (Campus & Christie, 2010)

and the true back azimuth in the infrasound system. EM radiation is not deflected by the wind, so the observed back azimuth is correct.
Another difference is maximum detection distance. The infrasound signal will damp over a certain distance. The EM radiation does not have this problem. With 7 EM sensors there is a coverage of the whole BeNeLux [14].

Although it would seem that for lightning detection EM radiation might be a better option, when the two systems (FLITS / KLDN) are compared, they do not give the same values of detection. Which system gives the right amount of lightning discharges? That is still unclear [3]. A different system with a different measurement technique may be used to validate the two EM detection systems. This system is the infrasound measurement technique. So it is independent from the other two detection systems. With this technique it should be possible to validate the two lightning detection systems.

1.5 Research on lighting detection with infrasound

A lot of studies about lightning were done between 1960 and 1980. In that time two mechanisms were suggested to explain how sound waves were generated by lightning discharges. *Few* (1969) was one of the first to suggest that lightning and the expansion of air have a direct effect on each other. The expansion of air creates the audible part of thunder [15]. *Holmes et al.* (1971) researched the power spectral measurements. In this study, they analysed 40 lightning events by the power spectral method. They concluded that other mechanisms are responsible for the creation of infrasound [16]. This study also showed that lightning has a frequency range of 10 to 200 Hz [15] [16] [17]. It shows that the audible signal first reaches the measurement station. This signal has a frequency

range between 50 and 200 Hz. This signal is followed by several pulses with a frequency that is lower than 20 Hz. Also they showed a difference between cloud-to-cloud (CC) and cloud-to-ground (CG) discharges. CC has a discharge with a mean frequency peak of 28 Hz, while a CG discharge has a peak at 50 Hz [16]. Besides of that, there is also a difference in total acoustic energy. The CG discharge has a higher total acoustic energy than a CC discharge [16].

The study of *Dessler* (1973), original *Wilson* (1920), explains how a electrostatic field produces a decrease of pressure inside the charged region of the cloud. In this region the charge is removed. Here the infrasound signal comes from a horizontal charged layer. Afterwards the signal will be radiated almost straight up and down. In this model the signal can only be measured if the sensor is placed directly below or above the charged layer. The model gives a suggestion that a rarefunction pulse is detected first. This is due to decompression. This could be followed by a positive pulse, the compression [12]. The model gives also an estimation of the amplitude and the peak frequency is given. The peak frequency has a range of 0.2 - 2 Hz [12]. *Dessler* (1973) has created a model. When it is compared by observations, it looks that the rarefunction phase amplitude is much larger than the compressional phase [18].

Lightning channels are first characterized during the 1970s - 1980s. In those studies they used acoustic arrays for the analysis of the thunder records. In the 70s - 80s they use a 30 meter side network, with a cross correlation technique. Few (1968, 1970) succeed to reconstruct the geometry of several discharges. The studies of *Few (1968, 1970)* showed that discharges present an essential horizontal expansion in the thundercloud [19]. The acoustic reconstruction of lightning is compared with photographs of the events by *Few and Teer, 1974*. The authors found a good agreement between the acoustic reconstructions and the photo's. This is only when the discharges are visible. When they look to cloud-to-ground discharges, they can say something about the vertical development of the return stroke. The length of this stroke is about 2 to 3 kilometers high. The acoustic reconstruction showed that the cloud-to-ground channel is still present in the cloud, but not visible for the optical devices. The same study insist the importance of knowledge of the local wind. This knowledge has to taken into account by a ray propagation. With a ray propagation program it is possible to calculate the 3D location of the source [20].

The horizontal development of a lightning strike in the cloud was confirmed through statistical studies of the reconstructed acoustic source by *Few and Teer, 1974* and by *MacGorman et al. (1981)*. This last study, showed 3D maps of acoustic sources from thunder. Besides of that, they analysed the statistical distribution of height of the reconstructed sources. *MacGorman et al. (1981)* found that acoustic sources were allocated in either one or two layers of the thunderstorm which they analysed [21].

For the last 20 years there were a lot of new studies about thunder localisation with infrasound. Those studies have the benefit that there was a development of the lightning localisation based on electromagnetic detection system like FLITS/KLDN at KNMI. These systems became in use since the 1980s.
There is also a new interest to acoustic reconstruction of the lightning channel. The acoustic method results can be compared with reconstructed geometries of discharges.

These are provided by high resolution electromagnetic detection network, for example a Lightning Mapping Array (LMA) [22]. The great challenge of this comparison is that the data is coming from different technologies. An acoustic source cannot be necessarily associated to a very high frequency (VHF) electromagnetic source (table 1

A pilot study is done at KNMI by *Holleman et al.,* (2006). Here they try to validate KNMI lightning detection systems which are based on electromagnetics. Several methods were done and one of them was with infrasound detections. In a frequency band between 1.0 and 20.0 Hz several features are observed. These features are refered to electrical discharge and thunder. The observed events correlate well to thunderstorms in time and bearing which are detected by the KNMI lightning detection system. *Holleman et al.* (2006) found that infrasound could be identified till at least 40 kilometers [4].

Different studies (*Assink et al. (2008), Farges and Blanc (2010)* and *Chum et al. (2013)*) compared the acoustic signals of lightning against the electromagnetic ones[5][6]. *Assink et al. (2008)* uses two infrasound array that can detect thunderstorm which are in the region of the infrasound array [23] [5]. They found a correlation between cloud-to-ground discharges as detected by the SAFIR (FLITS) system and the infrasound array. This good correlation was found up to 50 kilometers from the infrasound station. Furthermore there was found that there was a difference between the theoretical and the observed back-azimuth of $4.6 \pm 3.2°$[5].

Farges and Blanc (2010) found a good correlation between data of an infrasound array and the Météorage system (KLDN) with in 150 kilometers. A low detection efficiency of 5% is associated with to the notion that subsequent strokes are measured as one. While the infrasound signal can last for 10 seconds. This can lead to miss detections. If the distance of the lightning is to large, > 60 km, it can not directly associated with infrasound signals[6].

Gallin et al. (2016) make a coupling between three different systems. The Lightning mapping array (LMA), the European Cooperation for Lightning Detection (EUCLID) network and acoustic detections. The acoustic detections are infrasound and audible sound. They found when a lightning discharge strikes at more than 40 kilometers away. It could not be measured by the acoustic system. They also looked to the elevation angle of the signal. This elevation angle is correlated to the apparent velocity, c_{app}. In this study they found a good correlation between the LMA and the acoustic detections especially when the source is closer than 30 kilometers and for a elevation angle between 10°and 70°. Furthermore, there are no detections in the acoustic signal with a elevation angle smaller than 5°[22].

The last study is from *de Vos, 2015*. This study tried to do cross-baring with two infrasound arrays. This was very difficult because one array has less detections than the other array. Furthermore had the electromagnetic system much more detections than the infrasound array. Besides of this there is an uncertainty where exactly the source of the infrasound is by a lightning discharge. Furthermore, only linear propagation of the waves was done because there was no propagation model available. With this cross-bearing she found a probability of detection (POD) of 5.5% [3].

1.6 Research on lightning detection with EM

Lightning detection systems are hard to validate. Because a large ground truth dataset reference is hard to obtain. Various studies have been done in which the relative performance of several systems are determined. This is done by comparing datasets to one another or a differently get ground truth dataset. To get an idea of the relative performance of FLITS and KLDN, some relevant previous papers are used.

In a study that is carried out at KNMI, the CG data of FLITS/SAFIR has been validated. This is done by lightning related damage reports in The Netherlands from the NS (Dutch railways). The dataset covers a period from 2001 to 2006. The location and time of the lightning damage is used as a ground truth reference. In the case where the NS recorded a flash coincides with a stroke as reported in FLITS, in the matching and time area it is labeled as a hit. The POD was calculated by dividing the number of hits from FLITS by the total amount of damage reports by the NS. The averaged POD was $57 \pm 3\%$ [24].

Druë et. al (2007) studied the relatieve preformance of the SAFIR network against the BLIDS network. BLIDS is a part of the EUCLID network. Like BLIDS the KLDN network is derived from the sensors in the EUCLID network. BLIDS is used by the German weather service for the nowcasting of thunderstorms. The dataset was from May 2003 till December 2004 and the study area was a large area of Germany. The total lightning POD of SAFIR out of BLIDS is 60%. The other way around, so the total lightning POD of BLIDS out of SAFIR is 21%. These numbers suggest that SAFIR is more sensitive to the total lightning than BLIDS. The difference is due to the SAFIR network detects more CC lightning. But when they looked to the CG lightning, BLIDS performs better than SAFIR. Besides that, SAFIR seems to misclassify the CC lightning as CG lightning [25].

Another validation is done by Poelman et. al (2013). They used high speed camera images as a truth reference. With these images they want to validate the SAFIR, EUCLID and ATDnet system. The flashes were recorded on 3 days of August 2011 in Belgium. With those high speed camera images, individual strokes of the same flash are registered. Strokes will follow the same path of a single flash. The location accuracy could be determined as those strokes should be localized in the same location. Here the ground truth is found with the pictures. Now the detection efficiency could be found by calculating how much actual strokes are found by the detection system. Remark that FLITS is an updated version of the SAFIR network [26].

The SAFIR system uses Time of Arrival (TOA) with magnetic direction finding. This system has a detection efficiency with strokes of 64% and with flashes of 92%. This means that it misses some strokes, but the detection of lightning is quite good. The location accuracy of the detection system is 1.0 kilometers. When only the output of the VHF sensors of SAFIR is examined, it becomes significantly worse. The location accuracy will than be 6.1 kilometers. The ATDnet has a detection efficiency of 58% for the strokes and 88% for the flashes. The reason for this relative poor performance is due to a low detection efficiency on one of the three days. On that day the thunderstorms occurred during night. This has a negative effect on the performance of ATD. The location accuracy is the

	Stroke RDE(%)	**Flash RDE(%)**		**Stroke RDE(%)**	**Flash RDE(%)**
MTRG out of SAFIR	28	37	SAFIR out of MTRG	34	46
MTRG out of ATDnet	26	34	ATDnet out of MTRG	47	80
ATDnet out of SAFIR	27	60	SAFIR out of ATDnet	18	32
MTRG' out of ATDnet	40	57	ATDnet out of MTRG'	39	69

Table 2: Relative detection efficiency (RDE) values from Poelman et. al (2013)

same as SAFIR, 1.0 kilometers. The best performance is of EUCLID. Here the detection efficiency is for strokes 84% and for flashes 100%. The location accuracy for EUCLID is 0.6 kilometers, a bit less than the others [27].

A different study of Poelman et. al (2013) gives us the preformance of a Météorage dataset is compared with SAFIR and ATDnet. The Météorage dataset is the same lightning detection network as KLDN. A separation is made between the total lightning detection of Météorage and the low frequency detections of SAFIR. This detections are mostly the CG strokes. The detections were recorded in Belgium in the period of May till September 2011 and 2012. A hit is defined as two detection systems register lightning within a predefined temporal and spatial distance to each other. In this study all systems are used as a ground truth. Earlier was the POD described, but in this study the relative detection efficiency (RDE) is used. RDE is the percentage of hits between two datasets as part of the total detections. This total detections is used as the truth reference. The results are stated in table 2 Here the total lightning of Météorage is stated as MTRG'. MTRG are only the cloud-to-ground detections of Météorage [27]. A low RDE value could caused by a poor detection. An other reason could by a high false alarm ratio in a other system because they are all used as ground truth [26].

Another study that is carried out at KNMI, is an intercomparison of the FLITS and KLDN with ATDnet lightning detection systems [3]. The dataset which is used is from January 01, 2010 till October 31, 2014. From this intercomparison there state that FLITS detects a small amount of cloud-to-ground discharges and likely misclassified CG detections as CC detections. When the comparison is done between KLDN and ATDnet, which is expected to only detect CG. The fraction of ATD out of KLDN for total lightning is larger than for cloud-to-ground. This indicates that ATD detect more cloud-to-cloud as expected, or KLDN misclassified cloud-to-ground detections as cloud-to-cloud detections. The misclassifications occur in both systems, not only in FLITS, but also in KLDN. But the number of misclassifications of FLITS is much higher than of KLDN. The KLDN preformance of the cloud-to-ground detections is probably better than FLITS [3].

1.7 Outlook thesis

In this thesis there will be looked to validate the different lightning detection systems. The outline for this thesis will be as follows. Section 2 will describe the theory and the method of the detection and propagation of infrasound. Furthermore, there will be described which NWP model there will be used in this thesis. After that I will describe the 3D ray propagation model and the ray damping model. The 3D ray propagation model is first done for a toy atmosphere and later for a atmosphere of HARMONIE. Section 3 gives us the case studies of October 01, 2006 and July 27, 2013. With the coupling between KLDN, FLITS and infrasound data. And finally in section 4 a summary of this thesis and addresses the research objectives is stated. To which extent infrasound can be used to validate the EM detection system. After that the shortcomings will be discussed and the possible further research in this field.

2 Theory and method

In this chapter, the following methods are discussed:the measurement system, the Fisher ratio and the slowness vector. Furthermore the propagation of infrasound is discussed in more detail. In this part the different aspects are analysed: equations for a 3D propagation model, the different NWP models in order to decide which model gives the best meteorological parameters.

At first there will be looked at the detection part. This will include the measurement system, the Fisher ratio and in the end the slowness vector. After that we go through the propagation of the infrasound. At first which atmospheric conditions play a role at the propagation of infrasound. After that there will be explained what the equations are for a 3D propagation model. In the end we go through the different NWP models, to look what is the best model to give our meteorological parameters in our propagation model.

2.1 Detection system

Sound waves are measured by the KNMI microbarometer. This microbarometer is installed at several infrasound arrays. We will only use the array at De Bilt (DBN), which has six array elements, see figure 1. The barometer is very sensitive and can measure small air pressure fluctuations up to 10^{-2} Pa.

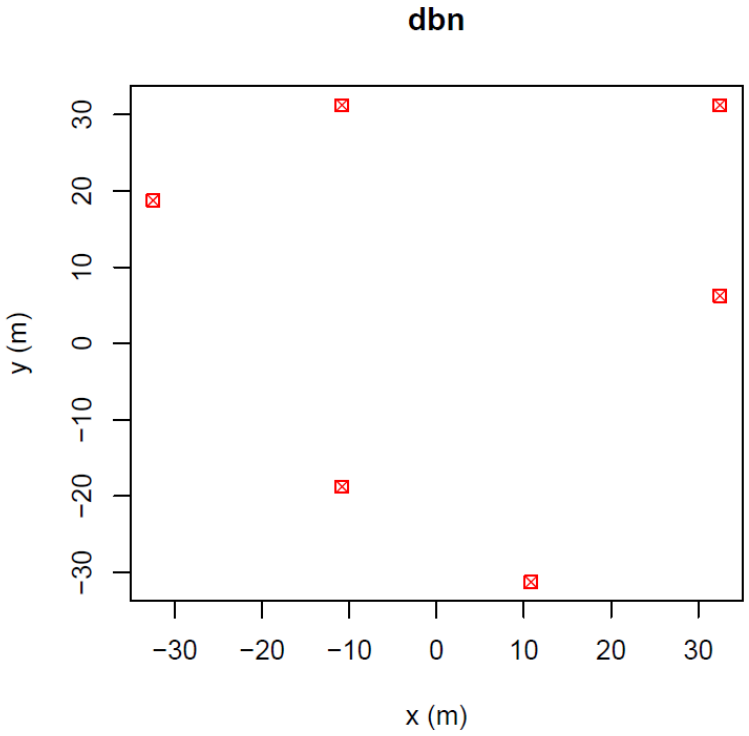

Figure 1: The infrasound lay-out of the array in De Bilt.

The microbarometer measures the pressure difference between the pressure of the sampled atmosphere and the reference pressure. This reference pressure is in the backing volume, see figure 2. Due to a capillary the microbarometer is only measuring pressure fluctuations with respect to the ambient air pressure. The lower frequency cut-off is determined by the acoustical resistance of the capillary. This acoustical resistance is determined by the diameter and length of the capillary. The relaxation time of the instrument is 500 s or $2{\cdot}10^{-2}$ Hz. So the lowest measured frequency is $2{\cdot}10^{-2}$ Hz. If the pressure fluctations period is larger than 500 s it leaked back towards the atmosphere. The atmosphere is sampled at a minimum rate of 40 Hz.

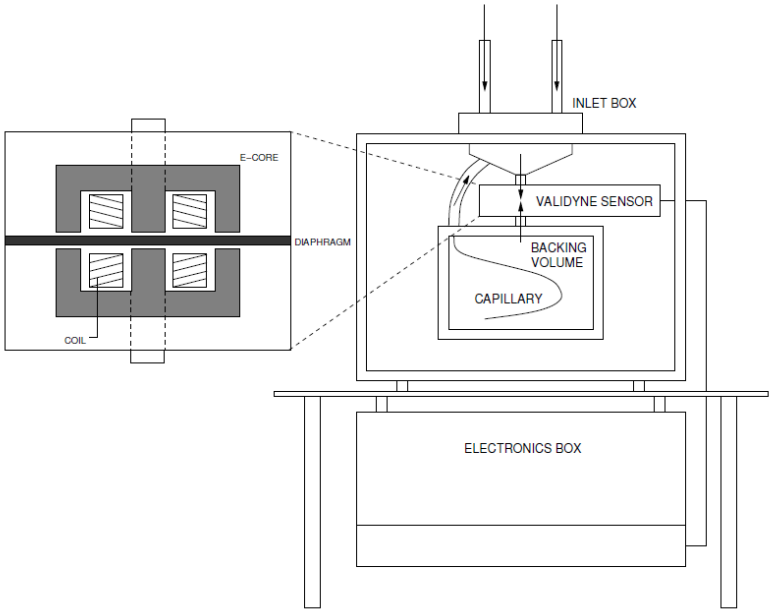

Figure 2: An overview of the KNMI microbarometer. The pressure fluctuations are measured by the Validyne sensor. The atmosphere is sampled through the inlet boxes, six in total. To get a differential sensor a backing volume is installed. In this backing volume, there is a capillary. This capillary "leaks" at a very low frequency pressure fluctuations back to the atmosphere [9].

The capillary is inside a thick walled backing volume, so the temperature will be stable. The instrument is inside a PVC box. This box stabilizes the instrument's calibration and protects it from the elements. The box has six openings where porous garden hoses are mounted, to reduce the wind noise. With this porous garden hoses the wind is now sampled over an area instead of a point. While the wind is incoherent over a small area and sound waves are coherent, this will improve the signal-to-noise ratio.
For a more detailed description of the instrument see [9].

2.2 Atmospheric conditions on infrasound

When propagation of infrasound is considered there is one important equation, the speed of sound equation. In this equation the sound speed is related to the temperature of the atmosphere. Besides this, the wave can go with the wind or against the wind. When it goes with the wind, it will go faster. When it propagates against the wind, it will propagate slower. The effective sound speed covers these two effects in the following equation [28]:

$$c_{eff}(z) = \sqrt{\gamma RT(z)} + \overrightarrow{w_{uz}}(z) \cdot \hat{n} = c_T(z) + w_a(z) \tag{1}$$

Here, $\gamma = 1.4$ and $R = 286.9$ J kg^{-1} K^{-1} are the ratio of specific heats ($\frac{c_p}{c_v}$) and the specific gas constant for dry air. $T(z)$ is the temperature profile in the vertical and $\overrightarrow{w_{uz}}(z) \cdot \hat{n}$ is the horizontal wind in the direction of propagation. In normal atmospheric conditions the temperature decreases with altitude in the troposphere. Under this condition the sound wave bends upward while it travels in the horizontal. The increase of effective sound speed could be caused by an increase in wind, temperature of a combined effect. A combined effect is the most common. Refraction follows from Snell's law and will bend the infrasound back to the surface [8].

2.3 Slowness

Beamforming techniques allow for detection of coherent infrasound, Fisher ratio, section 2.4 and the estimation of the slowness vector p. This slowness vector describes the direction of propagation in three dimensions. With simple equations this vector could be converted into the azimuth ϕ and the apparent velocity c_{app} as (Evers, 2008):

$$p_x = |\overrightarrow{p}|\cos(\phi) \tag{2}$$

$$p_y = |\overrightarrow{p}|\sin(\phi) \tag{3}$$

$$\phi = \arctan\left(\frac{p_x}{p_y}\right) \tag{4}$$

$$|\overrightarrow{p}| = \frac{1}{c_{app}} \tag{5}$$

$$c_{app} = \frac{c_{trc}}{\cos(\theta)} \tag{6}$$

Trace velocity, c_{trc} is the horizontal projection of the propagation velocity vector $\overrightarrow{c}$. It describes the horizontal speed of a wavefront with inclination angle θ.

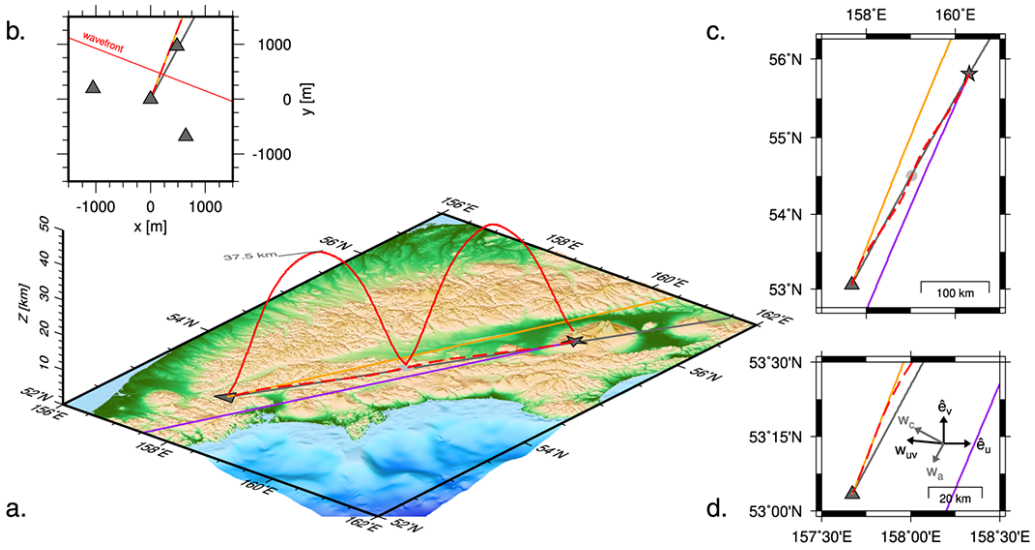

Figure 3: a) 3D map showing source (star) and detection (triangle) locations. Those two locations are connected with an eigenray (red line) and an horizontal projection (red dashed line). The purple, orange and grey lines represent the azimuth, back azimuth and theoretical back azimuth. b) An array element layout with the observed, theoretical and ray simulated back azimuth. c) A top view of figure 3a. The grey circle is the bounce moment at the ground from the signal. d) Zoom-in of figure 3c, showing the receiver area with the observed and theoretical back azimuth. [29]

In some studies, the back azimuth is used instead of the azimuth. Due to this change the detection array is now the point of reference. It is often found that there is a difference between the observed and theoretical back azimuth. These difference are present due to the influence of the wind and more specific the cross-wind, w_c. The difference in the back azimuth is shown in figure 3c. The difference in back azimuth is needed to let the true azimuth (grey line) and propagation azimuth (purple line) arrive at the receiver location. Hereby the propagation path is shown by the dashed red line. Furthermore, at the receiver location the observed back azimuth (orange line) does not point towards the source location. In only one case all those four lines are in line with each other. This is by a cross-wind of zero [29].

2.4 Fisher ratio

In this section the Fisher ratio will be described, which is used to identify infrasonic sources. The Fisher algorithm is proposed by R.A. Fisher; see Fisher (1948) [30]. His algorithm is based upon a statistical measure of coherence of several input time-series. The input is the time-series of the waveforms corresponding to the different array elements. The slowness vector $\bar{p}$, correspond to the back-azimuth and the apparent velocity of the event (as stated in section 2.3), is an important variable in the process. The Fisher algorithm tries to find the best slowness vector. This is done by aligning all waveforms forming a so called bestbeam. Melton and Bailey (1957) described the detection algo-

rithm in the time-domain. This approach will be described here [31].

The data of sensors are arranged in a matrix where the rows represent the number of sensors (N) and the columns individual time segments, bins (T). This together forms a $N \times T$ matrix. The value of each location in the matrix is analysed. The mean of each column is:

$$\bar{x}_t = \frac{1}{N} \sum_{n=1}^{N} x_{nt} \tag{7}$$

Here x_{nt} are time-shifted recordings. These recordings considered Gaussian distributed. This means that when summed over all time segments, the signal is enhanced with N. While the noise is enhanced with $\sqrt{N}$. This analysis uses the fact that the value at each location vary from the mean of the column with an error of ε_{nt} so $x_{nt} = \bar{x}_t + \varepsilon_{nt}$ and this mean vary from the average of the whole matrix, $\bar{x}$ by $\alpha_t = \bar{x}_t - \bar{x}$. The average of the whole matrix, the mean of all samples, is defined by Olson (2004)[32]:

$$\bar{x} = \frac{1}{NT} \sum_{t=1}^{T} \sum_{n=1}^{N} x_{nt} \tag{8}$$

To define the F-ratio, the total variance of the recordings is studied, which is the sum of the residuals [33]:

$$V_T = \sum_{t=1}^{T} \sum_{n=1}^{N} (x_{nt} - \bar{x})^2 \tag{9}$$

With some mathematics we get [32]:

$$V_T = V_W + V_B \tag{10}$$

with

$$V_W = \sum_{t=1}^{T} \sum_{n=1}^{N} (x_{nt} - \bar{x})^2 \tag{11}$$

and

$$V_B = N \sum_{t=1}^{T} (\bar{x}_t - \bar{x})^2 \tag{12}$$

From these equations V_W could be seen as the variance consist of both signal and noise. On the other side V_B consist only the signal power. The ratio over these two is equal to the snr^2. When we take a closer look at V_W, it stands for the variance inside a recording as it investigates each location with the mean of each column. V_B stands here for the variance between the recordings as it match the mean of each column with the grand average. V_T, the total variance, is split into two components to test the amount of variance in one variable is explained by the other one. Now we combine the equations that are mentioned above. The F-ratio is now defined as:

$$F = \frac{V_B / (T-1)}{V_W / T(N-1)} \tag{13}$$

This is rewrite in Melton & Bailey (1957) as:

$$F = \frac{T(N-1)}{N(T-1)} \frac{\sum_{t=1}^{T}(\sum_{n=1}^{N} x_{nt})^2 - \frac{1}{T}(\sum_{t=1}^{T}\sum_{n=1}^{N} x_{nt})^2}{\sum_{t=1}^{T}\sum_{n=1}^{N} x_{nt}^2 - \frac{1}{N}\sum_{t=1}^{T}(\sum_{n=1}^{N} x_{nt})^2} \tag{14}$$

Besides this equation Melton & Bailey (1957) has also derived a relationship between the singal-to-noise power ratio and the F-ratio. This relationship is important as it gives the snr^2 required for detection[31].

$$snr^2 = \frac{1}{N}(F-1) \tag{15}$$

In section 2.6 states an example of this time Fisher analysis. The data is from the DIA array, located in Deelen.

2.5 Detection algorithm

The processing is based on the detection of coherent signals. And following by an estimation of specific parameters to characterize the event. The parameters that have to be specified are:

- Back azimuth
- Fisher ratio
- Apparent velocity

Infrasonic signals are measured by the mircobarometers at a rate of 40 Hz and the detection algorithm find possible events of interest. This combination between measuring system and algorithm can perform in the time domain to find correlated signals. Two correlation detectors are frequently used in infrasound data processing, so called the Fisher detector (Melton and Bailey, 1957). The Fisher detector is based on the work by *Fisher* (1948) and analyzes the variance within measurements. After this *Melton and Bailey* (1957) initiated the F-ratio [30][31].

With this studies and the beam forming of section 2.3 and 2.4 we can make our algorithm. The parameters which are stated here above are calculated for a beam when a detection threshold is reached. The algorithm is build up from the following steps [9]:

- Read the raw infrasonic data. At first detrend the data and eventual merge the data, when there are several files from 1 station. A second order Butterworth band-pass filter, filters the data in frequency range between 1.0 and 10.0 Hz.
- The data is split into time bins. This happens when the time series became too long. A time series is too long if the time of the series is longer than the travel time of the wave over the detection system. The length of the time bin is station dependent. The time bin for DIA is much longer, the site is over 1.5 km, while DBN has a very small time bin, because the site spends no more than 80 meters. The bins have a 50% overlap so we are sure that a coherent wave, that travels over the array, is included in the bin.

- Make a slowness grid. With the slowness vectors (p_x and p_y) we can evaluate the apparent velocity and back-azimuth, see equations 2, 3 and 5. The grid has 50x50 points, with a slowness range of -0.005 to 0.005 s/m. With this interval, the apparent velocity range is between sub-acoustic and infinity velocities.
- Now with the equations of section 2.4 we can evaluate the Fisher ratio at every gridpoint in the slowness grid. Finally we get a gridpoint (p_x and p_y) with the highest Fisher number for that time bin.
- Point 4 is done for all time bins. So we have over time a whole set of slowness points. With those points we calculate the back-azimuth and apparent velocity. With this last step are the events characterized.

With this step we can now look how a waveform is travel over the array and go through the algorithm, to describe the event.

2.6 From waveform to detection

This section will give an example about signal detection and parameter estimation. Figure 4 shows 250 seconds of infrasound signal. The recordings are made by the microbarometer array at Deelen. The array in Deelen has 16 elements, at that moment only 13 microbarometers were operational. The recording started at September 4, 2007 at 20:03:18 UTC. Figure 4 shows 7 of the 13 waveforms. The program consider all 13 waveforms. The signal is filtered by a second order Butterworth band-pass filter. This filter is applied on the recordings, the frequency range is between 1.0 and 10.0 Hz. From this figure we see even more. The recordings between 140 and 150 seconds have the largest amplitude and show a high coherency. The recordings are processed using the F-ratio which is described by equation 14. The algorithm which is use to define the F-ratio is stated in section 2.5. The results of the detection and parameter estimation are given in figure 5 and 6.

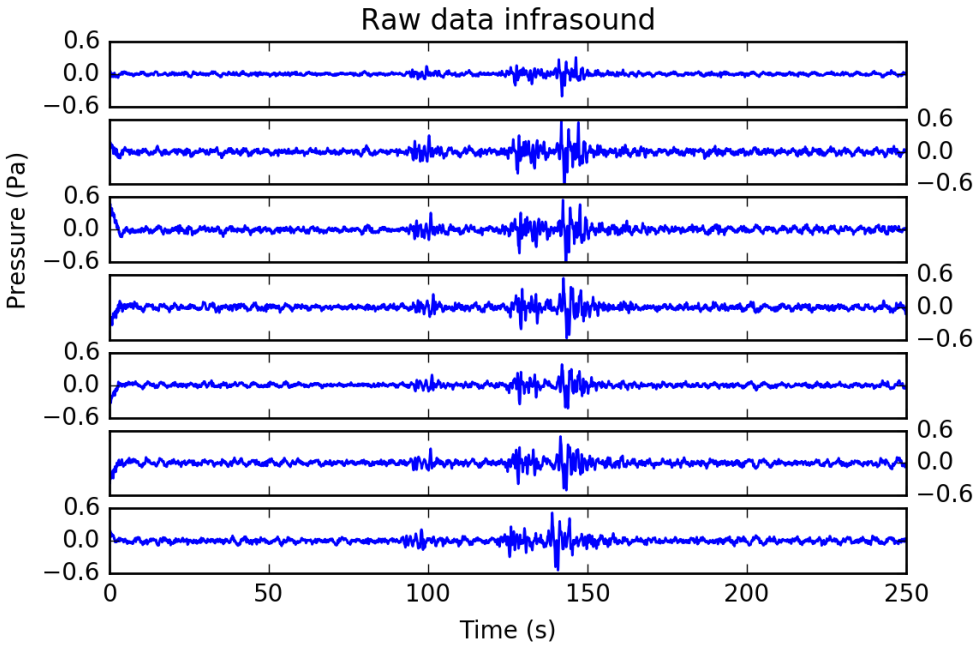

Figure 4: Band-pass filtered pressure data with a second order Butterworth filter between 1.0 and 10.0 Hz from the detection system. This are 7 waveforms from a single sonicboom. The time on the x-axis starts on September 4, 2007 at 20:03:18 UTC. The traveltime difference over the DIA array are clearly visible.

Figure 5 shows the Fisher ratio for each grid point in the slowness grid. This grid is for one time bin. The timebin has a length of 3.2 seconds. The length of the timebin is location dependent. I have chosen the bin where the Fisher ratio is the highest, so where the actual signal is. We can say that we have a coherent signal if the signal to noise ratio (SNR) is equal to 1. For the Deelen array the Fisher ratio has a minimum of 14. The maximum value of the Fisher ratio in this case is 102. This give a SNR of 7.7. In this figure we see also the corresponding slowness vectors with this Fisher ratio. p_x = -1.4·10^{-3} s/m and p_y = 2.4·10^{-3} s/m. With the equations 2, 3 and 5 we can estimate the important parameters. The back-azimuth is 300.3° and the c_{app} is equal to 360 m/s.

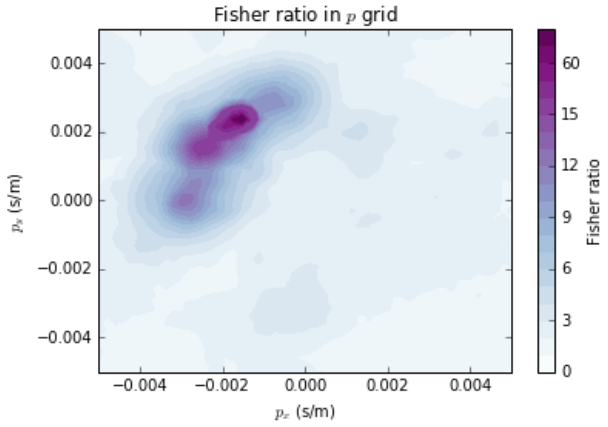

Figure 5: In this grid there are the two vectors of the slowness vector. With help of the Fisher ratio we can calculate what the apparent velocity and back azimuth of the signal is.

Figure 6 is the parameter evaluation. In the top panel shows the Fisher ratio. There is a first peak around bin 26-27 with a value of 61, the second peak is larger, with a peak at 102. Because this was a case of a fighter jet which goes through the sound barrier, we take the detection with the highest Fisher ratio as detection of the sonicboom. The second panel is the apparent velocity, c_{app}, with the apparent velocity and trace velocity we can calculate the angle of attack of the wave, θ. In this case θ is equal to 20°. The last frame is the back-azimuth, which is calculated by equation 4.

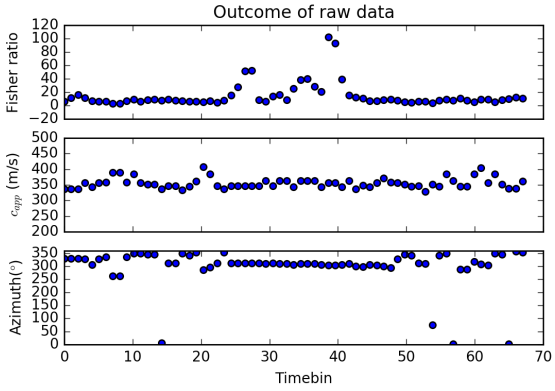

Figure 6: The results of the time domain F-ratio analysis. From the top to the bottom, the frames show F-ratio, apparent velocity and back-azimuth. All of them are as function of timein.

2.7 3D propagation equations

In section 2.2 stated an introduction about the Ray theory. This includes the effective sound speed approximation. In that approximation only the temperature and along-track wind is important. The cross-wind component is not taken into account in this approximation. This cross-wind component is the reason why 3D equations are needed. So in this part I introduce the ray theory for 3D propagation in a inhomogeneous medium, 'real atmosphere'. Here I will use Brekhovskikh and Godin (1999). The derivation and mathematics are stated in *Assink* (2012). With this approach we find the following system of 3D ray equations [34]:

$$\frac{d\mathbf{r}}{ds} = \frac{1}{c_g}\left(\mathbf{v}_0 + \frac{c}{\nu}\vec{\nu}\right) \tag{16}$$

$$\frac{d\vec{\nu}}{ds} = -\frac{1}{c_g}\left(\nu\frac{\partial c}{\partial \mathbf{x}} + \vec{v}_j\frac{\partial \mathbf{v}_{0,x_j}}{\partial \mathbf{x}}\right) \tag{17}$$

Here, $c_g = \sqrt{(v_{0,x} + \frac{c}{\nu}\nu_x)^2 + (v_{0,y} + \frac{c}{\nu}\nu_y)^2 + (v_{0,z} + \frac{c}{\nu}\nu_z)^2}$ and $\nu = \sqrt{\nu_x^2 + \nu_y^2 + \nu_z^2}$. $v_{0,x}$, $v_{0,y}$ and $v_{0,z}$ are the zonal, meridional and vertical winds. c is the local sound speed. $\vec{\nu}$ is the wavefront normal. $\mathbf{r}$ is the raypath. These ray equations is a set of coupled ordinary differential equations that could be solvind using a Runge-Kutta scheme to compute the ray paths. The following initial conditions are used [34]:

$$\mathbf{r}(0,\theta,\phi) = \begin{pmatrix} x_0 \\ y_0 \\ z_0 \end{pmatrix} \tag{18}$$

$$\vec{\nu}(0,\theta,\phi) = \frac{c_0\hat{\nu}(0,\theta,\phi)}{c_0 + \mathbf{v}_0 \cdot \hat{\nu}(0,\theta,\phi)} \tag{19}$$

$$\hat{\nu}(0,\theta,\phi) = \begin{pmatrix} \cos\theta\sin\phi \\ \cos\theta\cos\phi \\ \sin\theta \end{pmatrix} \tag{20}$$

Furthermore, θ is the inclination angle, the angle with the horizontal. ϕ is the declination, the angle with the north. In case of a reflection at the ground, $\theta_r = -\theta_i$, where r and i indicate the reflection and incidence. At the source, or, $s = 0$, the angels ϕ and θ must be specified as boundary conditions [34].

2.8 Toy atmosphere

In the coming sections I explain the creation of the 3D propagation program. The program has meteorological parameters input from the HARMONIE model. First we introduce a toy atmosphere and afterwards the meteorological parameters are one by one put into the model. So the impact of each parameter is clear .

2.8.1 Constant *T, u, v*

First the atmosphere is a constant temperature in all directions, 288.2K. There will be no wind. In figure 7 we see the temperature profile. It is very simple to calculate the

adiabatic / effective sound speed from equation 1. Because there is no wind, this equation is simplified by $c_{eff} = \sqrt{\gamma RT(z)} = c_T$. $\gamma = 1.4$ and $R = 286.9$ J kg^{-1} K^{-1}, as stated in section 2.2. T is constant over z, 288.2K. This gives a c_{eff} of 340 m/s.

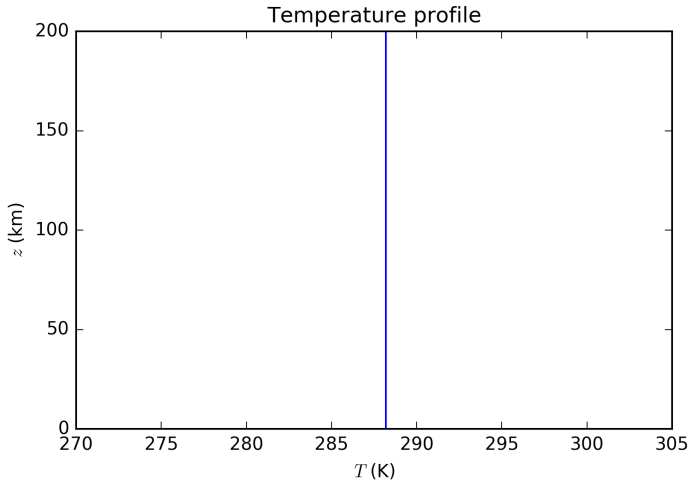

Figure 7: Temperature profile by a constant temperature in the whole atmosphere, 288.2K

We will expect with this profile that all rays that are shot into the atmosphere will not return to the surface. A ray will return when, as a first approximation, the effective sound speed at a certain height is higher than the effective sound speed at the height of the source. In figure 8 we see the ray tracer in this atmosphere. The source is at the surface and all rays are shot with an angle of 10° with the surface. Furthermore are the rays 10° apart of each other. In the real world sound wave is a continuous wave and not only waves at are 10°apart of each other. This is important to keep in mind for the next examples. When the source is at an certain height the rays which has an inclination angle between 181° till 359°propagates towards the surface and than bounce back into the atmosphere.

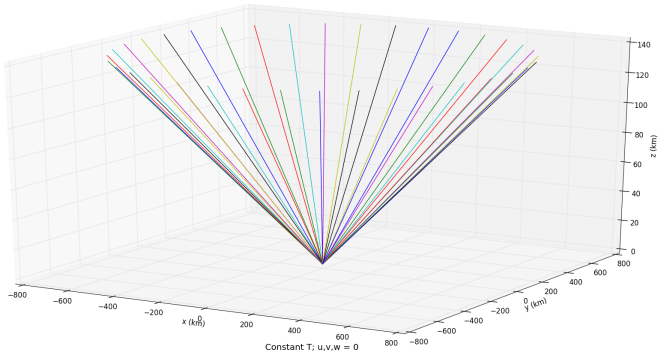

Figure 8: Ray tracing with a constant temperature in the whole atmosphere and a wind vector = 0. The rays are shot at an angle of 10° of the horizontal and are 10° apart of each other.

2.8.2 Variable T, constant u, v

The next step for our toy atmosphere is to apply a variable temperature. The temperature profile states in figure 9 and is based on *Lingevitch et. al 1999* [35]. The temperature at the surface is 288.8K. The profile is a polynomial fit tot the U.S. standard atmosphere (1976) [35]. The atmosphere has certain layers. From 0 till 10 km there is the troposphere. Above the troposphere there are the tropopause, stratosphere, stratospause and thermosphere. We know from equation 1 that temperature and sound speed have an one to one relationship. Furthermore will the rays bend back if the effective sound speed becomes higher than its sources height. In this case the height of the turning point is around 120 km, in the thermosphere.

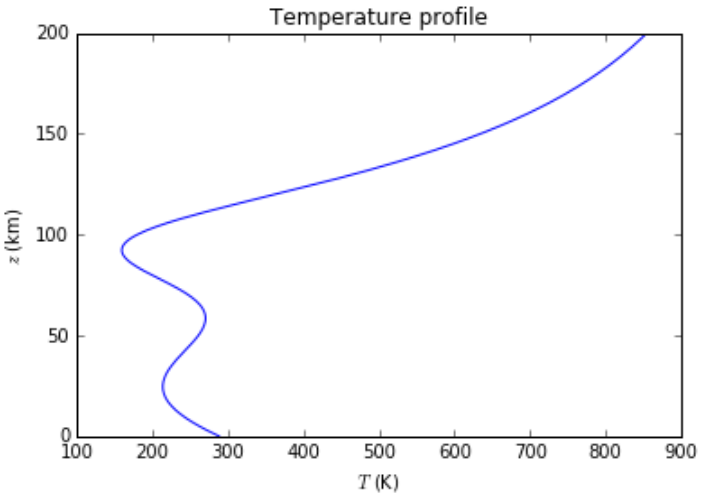

Figure 9: Temperature profile by a variable temperature in the whole atmosphere. The temperature at the surface is 288.8 K. [35]

Figure 10 shows the ray tracing for this case. In this figure there is no difference between the 3D ray equations and the effective sound speed approximation. This is due to the absence of wind. Like in the previous case the rays are shot in 10° of the horizontal and are 10° apart of each other. Note that in the 'real world' there is a continuous wave that propagates through the atmosphere. Because an atmosphere with no wind is far from reality we make now a toy atmosphere with wind.

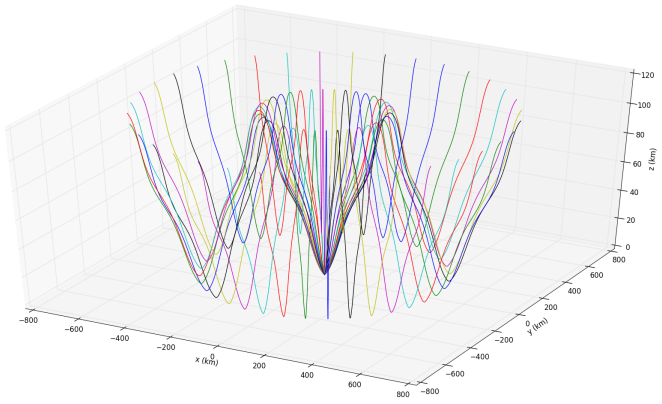

Figure 10: Ray tracing with a variable temperature, based on the profile of *Lingevitch et al. 1999*, and no wind field. The rays are shot at an angle of 10° of the horizontal and are 10° apart of each other.

2.8.3 Variable *T, u, v*

In this step we use the same temperature profile of figure 9 and add a zonal and meridional wind component. This wind component will be the jetstream which is at a height of 10 km. Figure 11 shows the wind component. It is an Gaussian function, with a total width of 20 km, above $z = 20$ km the wind is zero again. The wind maximum is at an height of 10 km and is 65 m/s, for the zonal component. For the meridional component it is 30 m/s. Now the wind and temperature is known we can make a first guess of the ray tracing. This will be done by the effective sound speed approximation. The effective sound speed is shown in figure 12. This is in the direction along the wind. In this direction we see that there is now an increase in effective sound speed around 10 km. When we compare this with the previous case there is an huge difference. In the first case the rays were able to pass the increases of effective sound speed till an height of 120 km. Now the increase is due to the wind so large that the rays are enable to pass this increase. The effective sound speed at 10 kilometers will be larger than the effective sound speed at source height (the surface). So the expectations are that the rays which propagate along the wind direction will band back at a height of 10 km. When rays propagate against the wind there is a decrease of effective sound speed, so we expect that those rays will propagate to a height of 120 kilometers.

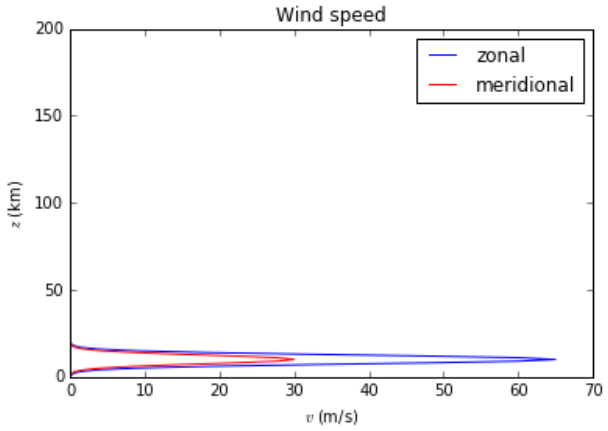

Figure 11: The zonal and meridional wind speed. It is a Gaussian function, with its peak to 10 km. The maximum zonal wind speed is 65 m/s. The maximum meridional wind is 30 m/s.

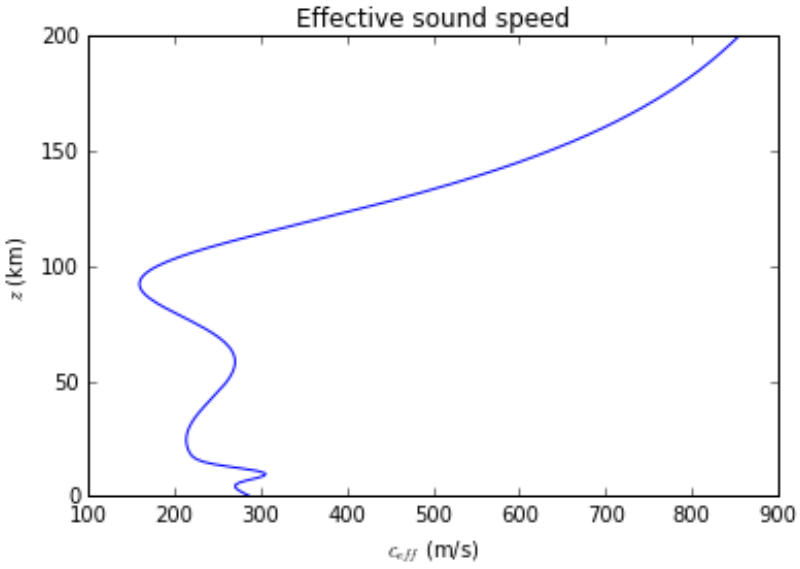

Figure 12: The effective sound speed is the adiabatic sound speed plus the along wind. This profile is in a direction of 50°. So the increase in effective sound speed is at a height of 10 km.

With this new profile of the atmosphere we did ray tracing, results are shown in figure 13. It is clearly to see what the wind causes on the ray paths. All rays that propagate in the direction of the wind will bend back at an height of 10 kilometers, as expected. This happens in a direction between 10° till 100°, so ± 40° of the main wind direction. In all other directions you see also the presence of the wind field at 10 kilometers height. The two rays which are not banded back (at 40 and 140°) are less steep around a height of 10 kilometers. While rays that are against the wind, around a direction of 270° are much steeper around 10 kilometers of height. This is due to a sudden drop in effective sound speed, so the difference will be higher, so the rays will be much steeper.

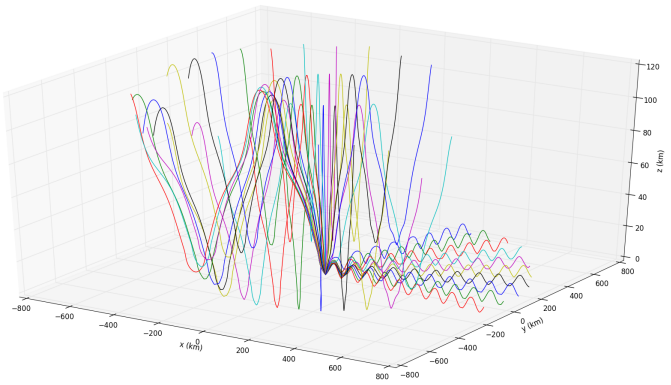

Figure 13: Ray tracing with a variable temperature, based on the profile of Lingevitch et. al 1999. There is now a Gaussian wind, with a maximum of 72 m/s at 10 kilometer height. The rays are shot at an angle of 10°of the horizontal and are 10°apart of each other.

Besides the rays by it self we are also interesting in the points where the rays are bouncing at the surface. Those points are important because the measurement stations are at the ground. So only when the rays are at the ground we can detect them. In figure 14 we see the bounce points of the different rays. When the ray goes against the wind, the first opportunity to detect the ray is around 400 kilometers away. While when the ray goes along the wind, it is after approximately 50 kilometers. This is a factor 8 closer. So when the detector stands along the wind, we have a greater opportunity to detect the sound wave. The reason that there are more detection points along the wind is, that the rays that goes along the wind, travels no further than 10 kilometers of altitude. While in the other way rays against the wind goes till an altitude of 120 kilometers. So there travel path so much larger than for rays which goes along the wind.

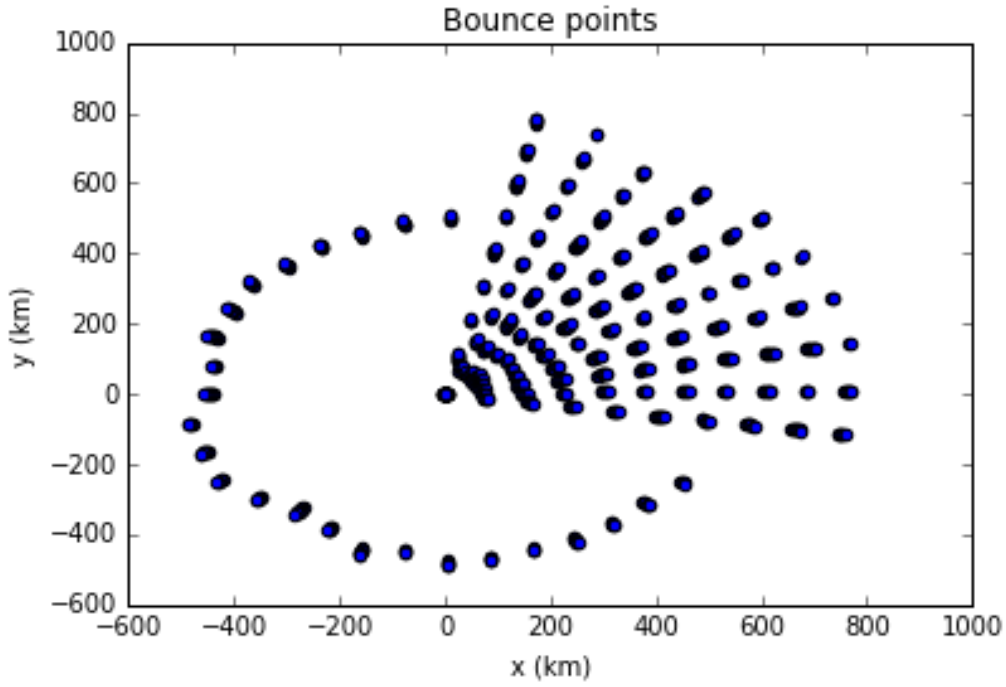

Figure 14: These are the points where the rays will hit and bounce at the surface. For a atmosphere with a variable T, u, v. (0,0) is the source of the rays. It is clear when the rays goes along the wind (positive x-axis) they bounce much earlier.

2.9 Weather data input

For the 3D propagation model we need input of the following meteorological parameters:

- Temperature
- Zonal wind
- Meridional wind
- Vertical wind

We need these parameters to get the correct path of the rays. At the KNMI we have three different models available: ECMWF, Hirlam and Harmonie. I will quickly go through all the three models and give in the end my conclusion about which model to use.

ECMWF

The ECMWF model is a global model. Which drives a lot of regional models like Hirlam or Aladin. It is mainly used for medium-range predictions, about 5 days ahead. It is probably the best weather forecast model, especially for the medium range. But in cases like extreme weather and convection it has its downside. This downside comes from that

the ECMWF model is a hydrostatic model. With a hydrostatic model it is unable to calculate the vertical velocities. These vertical velocities are critical to solve the convection. For example the turbulence scheme. The scheme is simple and has for example no turbulent kinetic energy (TKE) scheme in it. Furthermore is there a problem with the winter convection. It is generated above sea, but when the showers come over land the showers will disappear, which is not the case. But the biggest downside of the ECMWF model in our case is that convection is parametrized and is not calculated by the model itself. Moreover is that the resolution of the model is 16 kilometers in 2013, which is far too rough for this propagation model [36].

Hirlam

Hirlam is a regional model which gets its boundary conditions every three hours from the ECMWF model. The Hirlam model makes a weather prediction till 48 hours ahead, so it is a short range model. Like the ECMWF model, the Hirlam model is a hydrostatic model. This implicates that they assume that vertical acceleration are small. In convection this is not the case. The resolution of Hirlam is around 11 kilometers which gets us in a grey area about calculating convection. The area for calculating convection is between 200 meters till 15 kilometers. So in some cases the convection is calculated and in other cases it is parametrized. So it is very important with a propagation model, that a NWP model can calculate this[37].

Harmonie

Harmonie is a mesoscale model which gets its boundary conditions from the Hirlam model. Harmonie makes like Hirlam a weather prediction till 48 hours ahead. The most important advantage of Harmonie is its resolution, 2.5 kilometers. Due to this high resolution deep convection is fully calculated by the model. Moreover, this model is a non-hydrostatic model, so the besides that the convection is calculated also the vertical velocity is fully resolved. The reason that Harmonie is a non-hydrostatic model and Hirlam and ECMWF are hydrostatic models is very easy. The non-hydrostatic terms are only important with deep convection and in the mountain areas. So most of the time in The Netherlands an hydrostatic model is fine. But thunderstorms will only occur when there is convection, in this study Harmonie is the perfect model to work with [37].

2.10 Full 3D model with Harmonie

In figure 15 we see a full 3D model output. The meteorological parameters are provided from Harmonie. The parameters are from July 27, 2013 at 9:00 UTC. The rays are shot 10°apart from each other in the declination. In the inclination the angle is 20°and 340°. The height of the source is 500 meters. The rays that are shot in an angle of 340°came all to the surface, only some rays that are against the did not reach the surface. This does not mean that all rays which travels against the wind are not reaching the surface. This is always wind and altitude depended. For example, with a source at 100 meters of altitude, rays that travels against the wind will reach the surface. So it is very important that the height of the source is known. Unfortunately it is still unknown where the source of the in-

frasound is. It does not have to be a point source, but it could also be a line source. So the infrasound source could be come from 0 meters of height till the cloudbase for an example.

Furthermore what we see in the figure 15 is that at a certain point the rays which were propagating upward are reflecting downward. This is due to the fact that the effective sound speed becomes higher than the value at source height. When this happens the ray will deflect downwards, or in the other way upwards. In this model we can put the coordinates which comes from the lightning detection system FLITS or KLDN. When we run the program, a certain figure comes out of the program. Here we set the declination and inclination at 5°separation. After that we put in the coordinates of the infrasound array in De Bilt and the program gives us the eigenrays. This are the rays that we measure with the infrasound array. With those eigenrays we can determine the difference between measured back-azimuth and the theoretical back-azimuth.

The azimuth shift is very important to couple infrasound detections with the EM detections of FLITS and KLDN. The wind has no influence on the EM systems, so the measured back-azimuth is also the theoretical back-azimuth. For infrasound the wind has an influence. So the measured back-azimuth is wind shifted from the theoretical back-azimuth. The wind shift is place and time dependent because the wind is not every where the same.

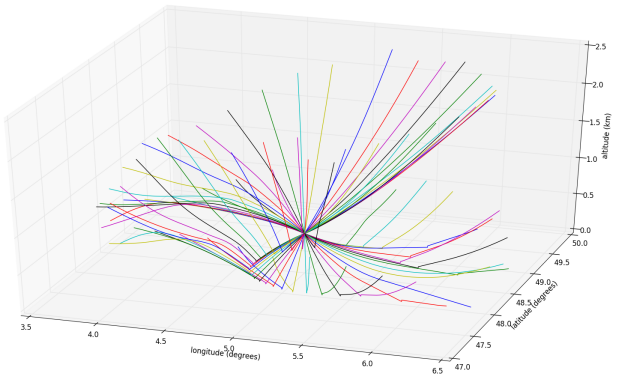

Figure 15: Outcome of the 3D propagation model. The meteorological input is from HARMONIE run 27-07-2013 at 9:00 UTC. The source height is 500 meter. The rays are shot 10°apart from each other. The inclination angle are at 20°and at 340°. All the rays that are shot from an angle of 340°reach the surface. Expect for those how travel against the wind.

In summary, atmospheric parameters (temperature, along-track wind) determine the effective sound speed and the trace velocity. While the cross-wind parameter determines the back azimuth difference. So, for infrasound observations we need sensitive tempera-

ture and horizontal wind measurements.

2.11 Damping of the signal in the effective sound speed approximation

In the previous section we found the equations to find rays. But the rays will not be measurable forever. At a certain point the signal is too damped to measure. The damping of the rays is evaluating by the transport equation. I will follow the steps which are defined by (Blom and Waxler, 2012). The amplitude of the signal, P_0 is a solution of the Zero-th Order Transport equation [38]:

$$\frac{d}{ds}\ln\left(\frac{P_0^2 D}{\rho_0 c_{eff}}\right) = 0 \tag{21}$$

Here D is the Jacobian transformation from Cartesian coordinates to ray coordinates, and ρ_0 is the ambient density. Now we assume that a spherical spreading at the source, one obtains the familiar transfer function [39]:

$$P_0 = \frac{1}{4\pi}\left|\frac{\rho(s)c_{eff}(s)\cos\theta}{\rho_0 c_{eff}(0)D(s,\theta)}\right|^{\frac{1}{2}} \tag{22}$$

The physical inputs in those equation are the effective sound speed with its first and second derivatives. These are not bases on the 3D equations. In this research the damping based on the effective sound speed is a good assumption.

One of the important things with infrasound is the damping of the wave. When the ray is too much damped we can not detect the wave. Like with the propagation the wind is very important. The largest difference in terms of damping is between a ray that travels along the wind and a ray that travels against the wind. In figure 16 we plotted the rays that travel along the wind (to the right) and against the wind (to the left). We have a source at an altitude of 1000 meters. All the rays are shot with a distance of 10°apart of each other. In this case the rays which travel against the wind propagates directly in the direction of the stratosphere. In this model we used the effective sound speed approximation. In a 3D model the rays are not directly propagating towards the stratosphere, but to get a picture how the damping is over the rays, this is good enough. In the troposphere the absorption is almost zero. So the damping is due to the geometrical spread [40][41]. In figure 16 we see that a ray which propagate along the wind is less damped than a ray that propagates against the wind. For the mean rays the difference is a factor of 1.5. This factor 1.5 does not hold up for the whole atmosphere. It is wind dependent and should always recalculated again. The wind field is a big player with ray tracing.

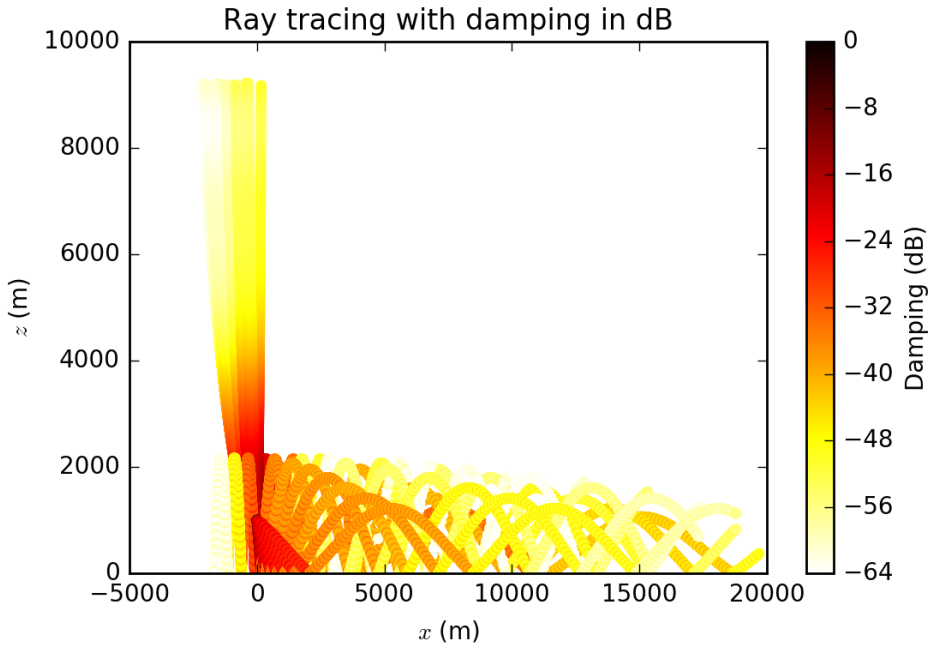

Figure 16: The rays are shot in 2 directions: along the wind (to the right) and against the wind (to the left). The source height is 1000 meters. The rays are shot with a seperation of 10°of each other. When a ray reach a altitude of 9,000 meters it is cut off. The colorbar shows the damping in dB.

3 Case studies

In this section we will look to two cases. The first case is at October 01, 2006. Due to the lack of data at that time, we will look global to the setting and asking questions what we will answer in the second case. The second case is at July 27, 2013. In this case we will answer the questions of the first case and several other questions which will come up.

3.1 Case 01-10-2006

This case is at October 01, 2006. In figure 17 we see the weather analysis at that day of 12 UTC. There is a low pressure system over South-East Ireland with an occlusion front around it. Between the occlusion front and the low pressure system we have several height troughs. The other systems in this case are not interesting and will not affect the Netherlands in the coming 12 hours. The occlusion front passes at 14-15 UTC over De Bilt. After the occlusion around 21 UTC a height trough will pass. At both moments there are lighting discharges which picked up by the infrasound array and the FLITS network. In the following subsection we will look to the difference between the FLITS network, which is driven by electromagnetic radiation and the infrasound network.

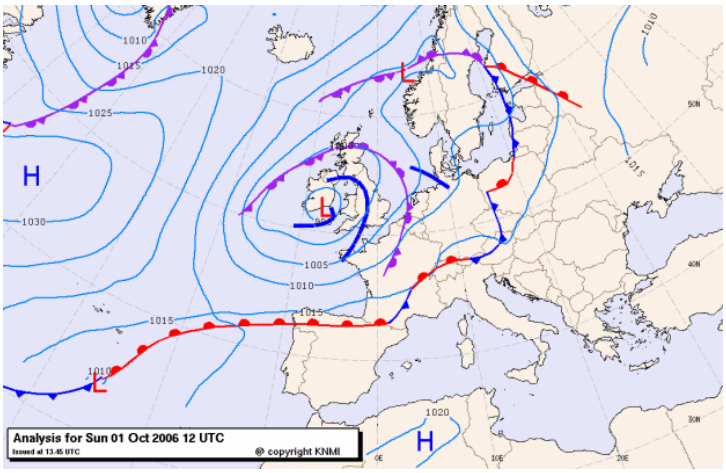

Figure 17: The weather analysis at 01-10-2006 at 12 UTC. Here is a occlusion at the Dutch coast, which past De Bilt 14-15 UTC. Further to the South-West there is a through which passes at 21 UTC.

3.1.1 Infrasound vs. FLITS

In this section we look to the difference between electromagnetic detections and infrasound detections. In figure 18 we see the infrasound detections in red and the FLITS detections in grey. In the first panel we see the back-azimuth of the signal. This is the only panel where also the FLITS detections are plotted because in the other two panels are infrasound parameters. In the second panel we see the apparent velocity and in the last panel the Fisher ratio.

In the top panel of figure 18 we see sound three thunderstorms passing by, at 02 UTC, 14-15 UTC and 21 UTC. In the FLITS and infrasound system we see the thunderstorms. But in the thunderstorm of 14-15 UTC we see it go further in time than the infrasound signal. We see this also in the thunderstorm of 21 UTC. Between 15 and 20 UTC FLITS detect a lot of lighting discharges while the infrasound array detect only a few. In the third and fourth panel we see that the apparent velocity and Fisher ratio is relative low. So the thunderstorm was relative far away. But what is the maximum distance of a lightning discharge what we can detect with the infrasound? This we will answer in the following case of July 27, 2013. In the lower two panels we see that when the apparent velocity increases, the Fisher ratio increases too. This is due to the distance of the discharge. The closer the discharge is at the array, how higher the apparent velocity and Fisher ratio. Furthermore the azimuth will shift 180°.

We can think that there are also lightning detections between 05 UTC and 14 UTC. But all those detections are noise. So not every detection at the infrasound array is a lightning discharge. It could also be something else. Some of these sources are stated in section 1.3. Other sources which are not stated in section 1.3, but are very important for this location are several tunnels and overpasses in all directions [42]. So not every infrasound detection is a lightning discharge. It could be another infrasound source. This is very important to keep in mind.

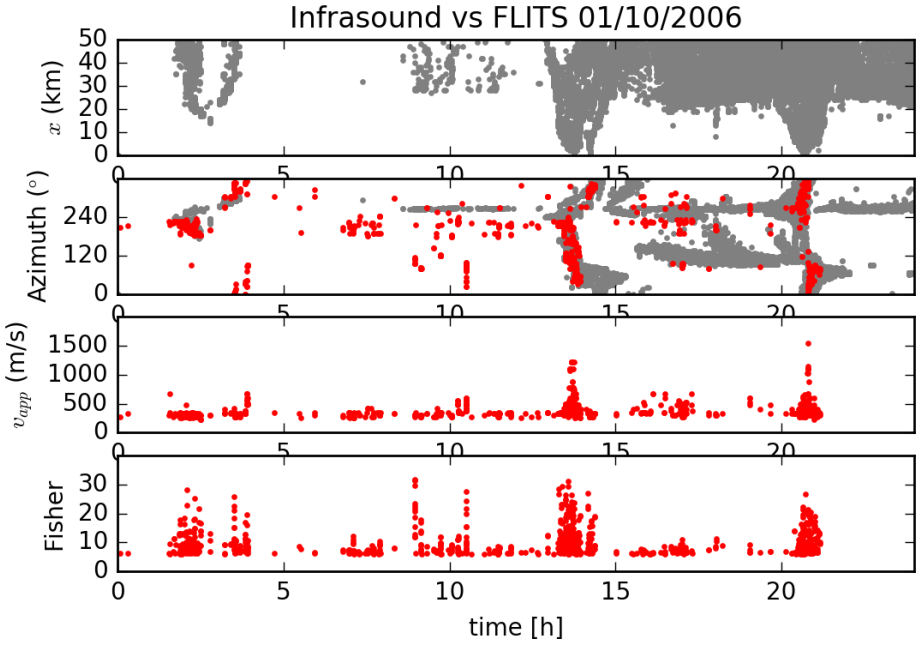

Figure 18: The red points are detections from the infrasound array and the grey points shows the detections of the FLITS system. The dataset is from 01/10/2006. The panels are from upper to bottom; distance, back-azimuth, apparent velocity and Fishre ratio.

3.2 Case 27-07-2013

3.2.1 Meteorological analysis

The second case is a clear summer convective case. The day of the case is July 27, 2013. In figure 19 we see the weather analysis of 06 UTC. This is a clear Spanish Plume case. Here warm, moist air is pushed in the direction of The Netherlands. In front of this moist air there is a easterly wind of 100°. In the moist air blows a southerly wind of 170°. The difference between the two different air flows is 70°. Hereby arises a convergence line. The red line in Northern France. This convergence line passes De Bilt around 9:45 UTC. This goes with a squall line which produces heavy rain and thunderstorms and large wind gusts up to 24 m/s or 87 km/h. In the Beaufort scale this wind gust is categorized in scale 9/10. We will go in to this squall line. And will look how the infrasound detection method stands against the FLITS and KLDN network. The period which we looked to is from 9:00 UTC till 11:00 UTC.

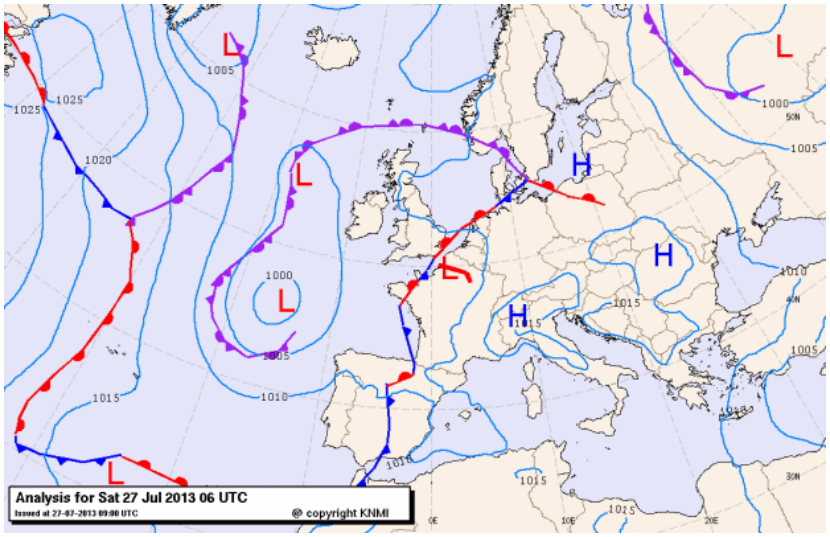

Figure 19: Analysis of 27-07-2013 at 06 UTC. Here is a convergence line in Northern France. This will pass De Bilt around 10 UTC.

In figure 20 we see all detections of the FLITS network between 9:00 and 11:00 UTC in a range of 80 kilometer from De Bilt. In figure 21 we see all detections of the KLDN network. When we compare both systems it is clear that the FLITS network has much more detections than the KLDN network, this is also stated by de Vos, 2015. Furthermore wee see the squall line coming from the south and passes De Bilt (the 'x' in the figures) around 35200 seconds after midnight. This is approximately 9:45 UTC.

Now we have the synoptic case described and lighting detections by the two systems we will look at the effective sound speed at 9:45 UTC at De Bilt. At the time when the squall line passes. At that time we have a wind from 170°with a speed of 11 m/s.

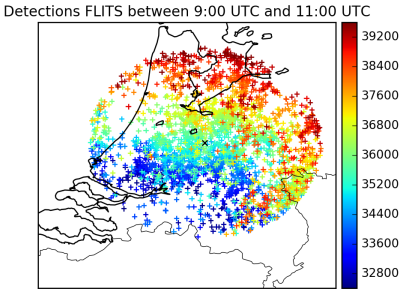

Figure 20: All lighting detections by the FLITS system between 9:00 and 11:00 UTC. With a distance of 80 km from De Bilt.

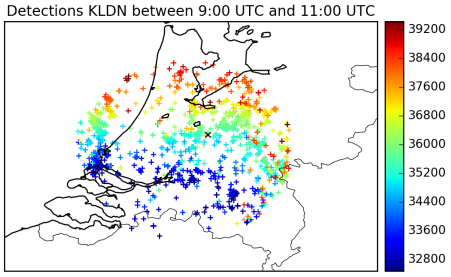

Figure 21: All lighting detections by the KLDN system between 9:00 and 11:00 UTC. With a distance of 80 km from De Bilt.

3.2.2 Comparison NWP models

All the meteorological parameters come from the HARMONIE weather prediction model (NWP). On the left of figure 22 side we have the output of HARMONIE and on the right side we have ECMWF output. The upper panel is the adiabatic sound speed, c. The middle panel is the meridional component of the wind speed, v, and the lower panel is the zonal component of the wind, u. The y-axis is between the surface and an altitude of three kilometers. Higher then this layer is not interesting for us because the infrasound will be too damped to measure. The x-axis is the latitude which goes from 51°N towards 53°N for the HARMONIE model. For ECMWF the x-axis is between 47°N and 56°N. This is due to the delay in the convergence line of ECMWF. The black dot represents De Bilt. We see a large difference between the HARMONIE and ECMWF output. In the HARMONIE output we see large difference in a small area, due to its high resolution. In the ECMWF output we see a more layered pattern, which is quite normal for a global model. The ECMWF model scores very good, but not on a scale with a convective modus as HARMONIE. HARMONIE scores well with convective situations, due to the non-hydrostatic model. ECMWF is hydrostatic, so it scores with convective situations less. In HARMONIE the convergence line is very well visible. Figure 22 gives the output from 9:00 UTC where the convergence line is in the region of De Bilt. The wind shift is recognizable due to the increase in in the meridional component of the wind and a drop in the temperature. This two parameters are very important of the propagation of the infrasound.

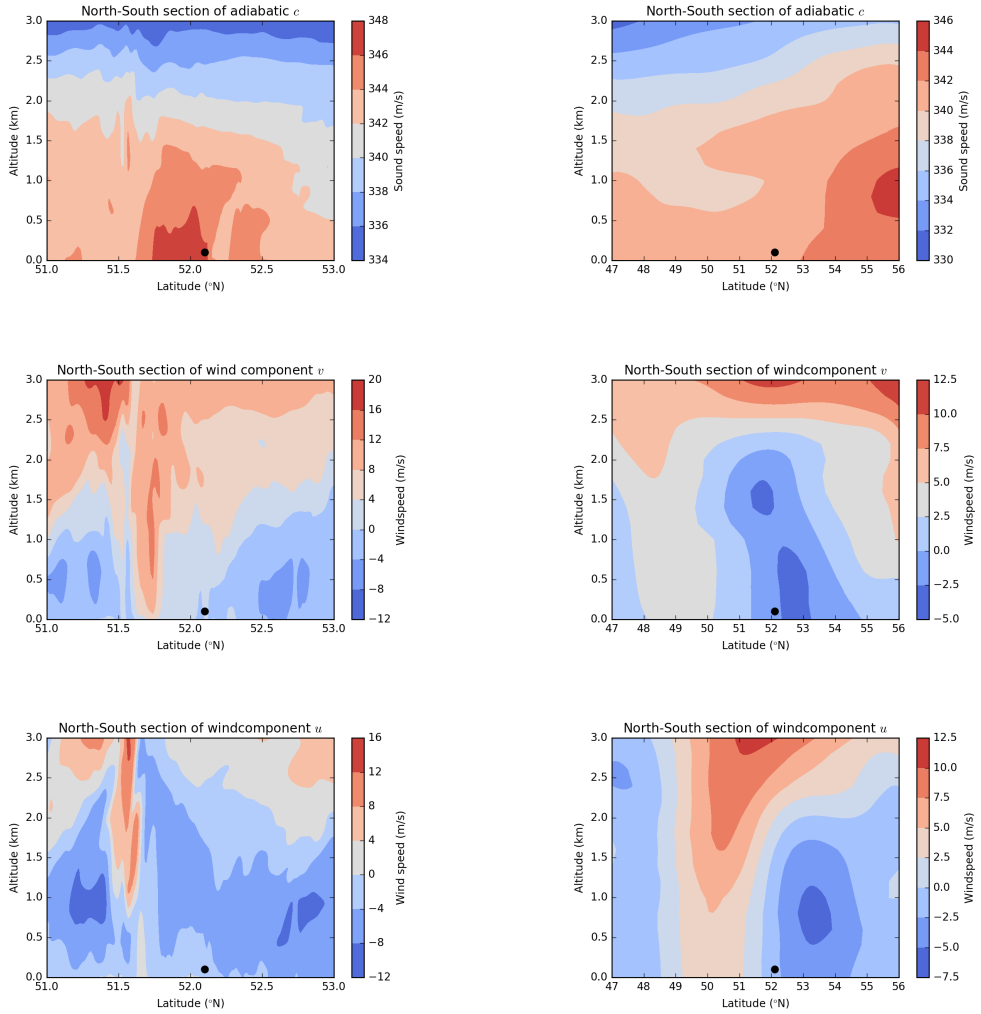

Figure 22: On the left side is the HARMONIE output and on the right side it is from ECMWF. The date and time for this output is 27-07-2013 9:00 UTC. All figures are a cross-section from North to South. And it goes from 50°N till 54°N. At the top figures there is the adiabatic sound speed, which is correlated to the ambient temperature. The middle one is the meridional component of the wind (v). The lowest one is the zonal component of the wind (u). The black dot in the figures are representing De Bilt. At the y-axis there is the altitude which goes till only 3 kilometers.

In figure 23 we see two different sound speeds, one adiabatic, red line, and one effective, blue line. The difference between those two is that in the effective sound speed also the wind is countered in, which could be seen in equation 1. When the effective sound speed is higher than the adiabatic the sound wave goes along the wind. From figure 23 it is clear that we have an south to southeast wind. So propagation towards the North are along

the wind and also propagation towards the west to northwest are easier to detect. So discharges that are to the south and east to southeast and within reach of 40 kilometers from De Bilt could be detect by the infrasound array.

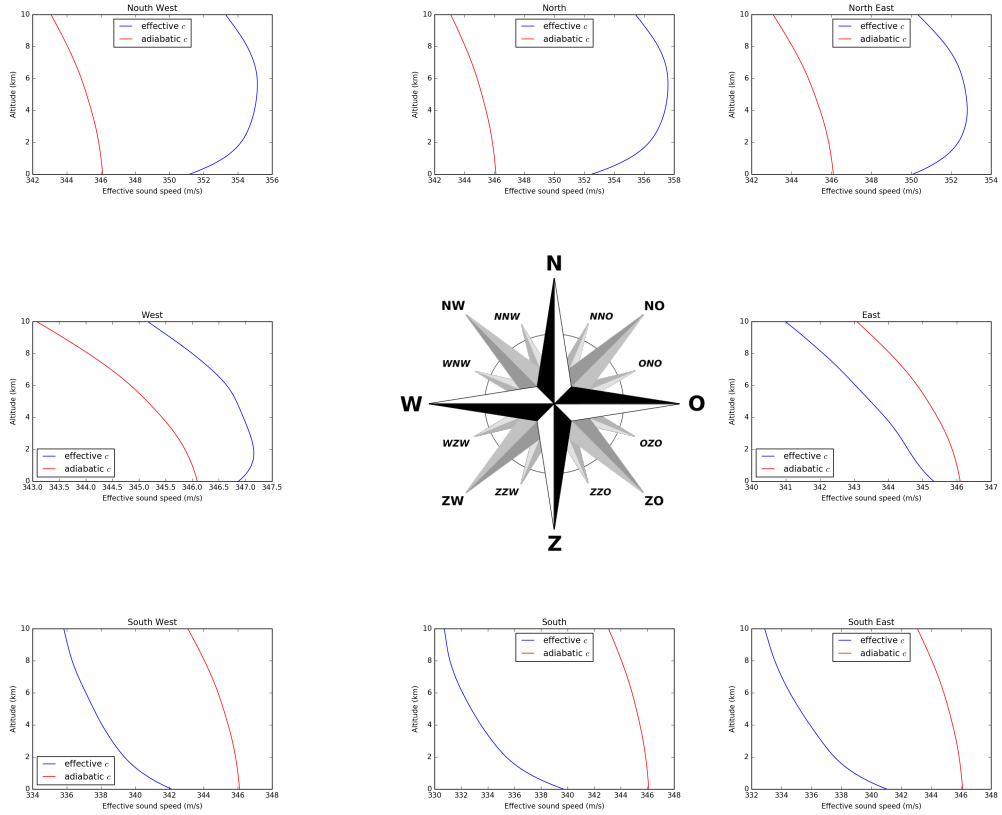

Figure 23: The adiabatic sound speed in red and the effective sound speed (adiabatic + wind component) in blue against height. The height is till 10 kilometers and this is due to our area of interest.

3.2.3 Accounting for propagation efficiency

When we will compare the detections from the north but also from the south we have to find a way so that we can deviate the wind out. When the ray travels along the wind, the ray comes further. When the ray travels against the wind, the ray comes less far. Now we take the ratio between the maximum effective sound speed and the adiabatic sound speed. We take as assumption that at the surface the wind is zero. If the effective sound speed is larger the ratio becomes < 1 and if it is smaller it becomes > 1. Now we multiply it times the distance and we have than the effective distance. Discharges which are along the wind are closer by and discharges which are against the wind are further away. In figure 24 we see the both detection systems with the effective distance. We see the dark color around 35000 s. Here is the thunderstorm over the De Bilt, so the

effective distance and the real distance are than very small. In figure 24 we see on the left side the FLITS network. Here are the pentagons cloud-to-ground (CG) discharges and the '+' are cloud-to-cloud (CC) discharges. FLITS has 24 CG discharges and 1719 CC discharges. On the right hand side there is the KLDN network. Also here the pentagons are CG discharges, the others are CC discharges. KLDN has 187 CG discharges and 131 CC discharges. The first thing that strikes is the difference in total between FLITS and KLDN 1743 against 318 discharges. Besides of that KLDN has a lot more CG discharges than FLITS. Almost all CG discharges by FLITS were also detected as CG discharges by KLDN.

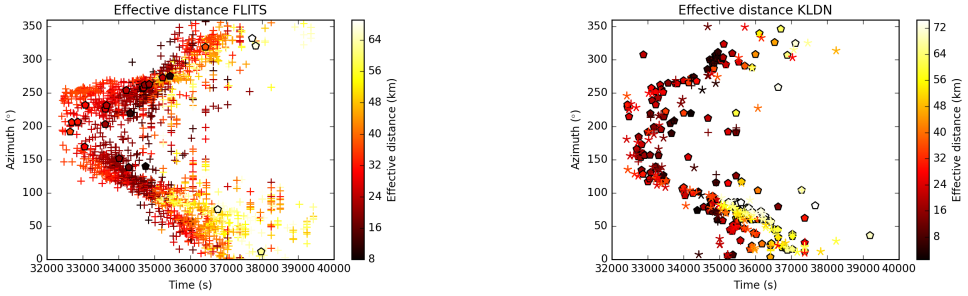

Figure 24: In the left frame all detections, in a radius of 50 kilometers from De Bilt, of FLITS are shown. The + are cloud-to-cloud discharges and the pentagons are cloud-to-ground discharges. On the y-axis there is the back-azimuth of the signal. On the x-axis is the time. The time is in seconds after 27-07-2013 0:00 UTC. The color represents the effective distance, ratio of maximum effective sound speed and effective sound speed at the ground, of the discharge. The right frame are all detections of the KLDN system. The + and pentagons have the same meaning. The asterisk are also cloud-to-cloud discharges.

3.2.4 Infrasound

Now the case is described we can look to the infrasound detections. The raw sensor data output states in figure 25, on the x-axis there is time in UTC and on the y-axis are the pressure fluctuations in Pa. We see that around 9:45 UTC the thunderstorm passes the sensor. At that time the pressure fluctuation is too large for the datalogger, around 400 Pa, and it clips for a couple of minutes. This is due to the dynamical range of the datalogger. After the convergence line has passed there is again a clear infrasound signal.

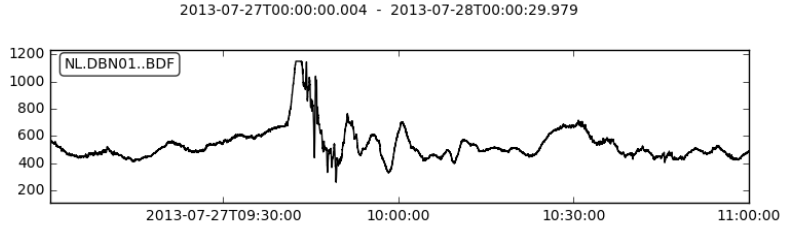

Figure 25: The raw output of array element 01. On the y-axis are Pa. On the x-axis is the time. The time goes from 27-07-2013 9:00 UTC till 27-07-2013 11:00 UTC.

All the detections between 9:00 UTC and 11:00 UTC are shown in figure 26. In the highest panel we see the apparent velocity, in the middle the Fisher ratio and in the lowest panel the back-azimuth of the signal. There are three remarkable points in this figure. At 34000 s, 35000s and after the 35000 s. Around 34000 s we have detections with a very high Fisher ratio and a high apparent velocity. Besides of this the back-azimuth also shifted from the south towards the north in this period. Those points, high Fisher ratio, high apparent velocity and a changing back-azimuth suggests that there were lightning strikes detected. In section 3.2.6 there will be looked to the detection around 34,000 s of those detections where lightning strikes or not. At 35000 s the sensor have not recorded a single detection (noise or lightning).

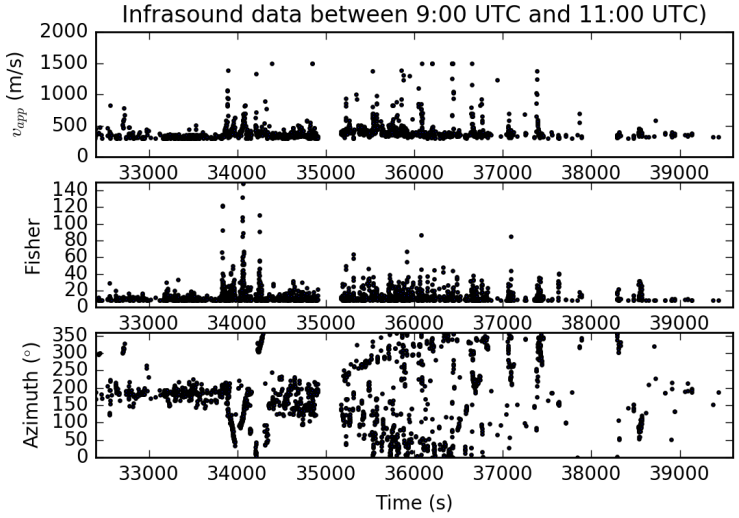

Figure 26: The infrasound data captured at the test field in De Bilt. In the first frame there is the apparent velocity. In the second frame there is the Fisher ratio and in the last frame we have the back azimuth. This is in a time frame from 09:00 UTC till 11:00 UTC. The convergence line passes De Bilt around 9:45 UTC (35000 s).

This is due to a very high pressure signal where the measurement system quits. This

was when the convergence line was passing De Bilt, around 9:45 UTC. After 9:45 or 35000 s the detections were in the east, west and north of De Bilt. So we see a characteristic line going from around 180°up to 360°or going down to 0°. After 36700 s the lightning discharges are too far from De Bilt that the infrasound system can not detected these signals. When we look to the figures 20 and 21 we can say that the thunderstorms goes over De Bilt around 9:45 UTC. In figures 27 and 28 there are the same figures as 20 and 21, but with infrasound (green points) plotted. A closer look to this we see the infrasound signal and the EM signal from FLITS and KLDN coming in at around 32000 s, with a back-azimuth around 200°. This back-azimuth stays till 35000 s (9:45 UTC). After this point the thunderstorm is moving over De Bilt so the back-azimuth will gradually shifting towards the North (0 or 360°). The pattern we see in FLITS as in KLDN and the infrasound signal. Not all infrasound points follow the points of KLDN or FLITS, these are likely noise or other infrasound sources. The points from 34500 s with an back-azimuth of 180 ± 20°are likely infrasound sources that come from De Uithof. At the De Uithof there are some sources that are wind driven. With a wind from the South it is possibly at those wind drive infrasound has reached the infrasound array. The other points that

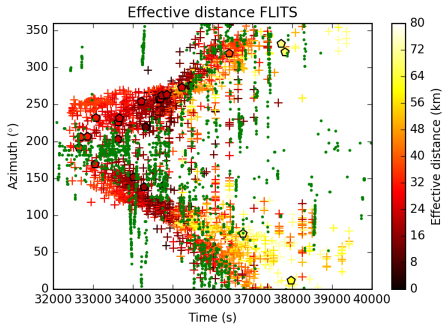

Figure 27: All detections, in a radius of 50 kilometers from De Bilt, of FLITS are shown. The + are cloud-to-cloud discharges and the pentagons are cloud-to-ground discharges. On the y-axis there is the back-azimuth of the signal. On the x-axis is the time. The time is in seconds after 27-07-2013 0:00 UTC. The color represents the effective distance, ratio of maximum effective sound speed and effective sound speed at the ground, of the discharge. The green points are the detections of the infrasound array.

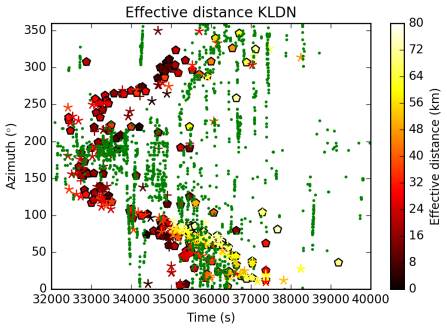

Figure 28: All detections, in a radius of 50 kilometers from De Bilt, of KLDN are shown. The + and asterisk are cloud-to-cloud discharges and the pentagons are cloud-to-ground discharges. On the y-axis there is the back-azimuth of the signal. On the x-axis is the time. The time is in seconds after 27-07-2013 0:00 UTC. The color represents the effective distance, ratio of maximum effective sound speed and effective sound speed at the ground, of the discharge. The green points are the detections of the infrasound array.

follow the points of KLDN or FLITS are likely lightning detections. When we looked to the wave characteristics, they are. What we can see here is that the infrasound detections followed the detections of FLITS and KLDN till an effective distance of 25 kilometers. It is better seen in figure 27 than in figure 28, but this is due to the density of detections. From *De Vos, 2015* we know that FLITS gives much more CC discharges, this is also the case here. Furthermore it gives a lot less CG discharges. This amount is much too

low. KLDN gives a lot less CC discharges when comparing with FLITS, but more CG discharges. This is very important because the infrasound is sensitive for CG discharges.

3.2.5 Back azimuth shift by the wind

Now we know that the infrasound detections follow the azimuth-time line of the EM systems, we look at the measuring back-azimuth at the detector. We have nine different discharges around De Bilt (DBN) and Cabauw (CIA). Figure 29 shows these discharges. The red '+' is the position of discharge which will be discussed. The other 8 grey '+' are different positions of discharges. The black line is the theoretical back-azimuth. This will be the back azimuth if there was no wind. The blue line is the measured back-azimuth and the red line is the ray path. The infrasound source is put at an altitude of 800 meters. The smallest azimuth error is 0.8°. This is the detection which is the closest to Cabauw. The ray with the largest azimuth error, 7°, has the most effect of the cross-wind. A small side note is that this ray has the longest ray path. So the wind effect is here the largest. Each discharge has its own azimuth error. It is important to calculate the azimuth error at each event. A 7°change in back-azimuth is not very much, but when a discharge is at a distance of maximum 40 kilometers, the error is 5 kilometers. FLITS has a maximum error of 1 kilometer and KLDN even 600 meter. When this is not taken into account, we will say that a detection at the EM system and a detection with the infrasound is not a match. But due to the wind effect this is a match. So it is important to take the wind effect into account. The 3D propagation model is able to calculate the back-azimuth error for each point.

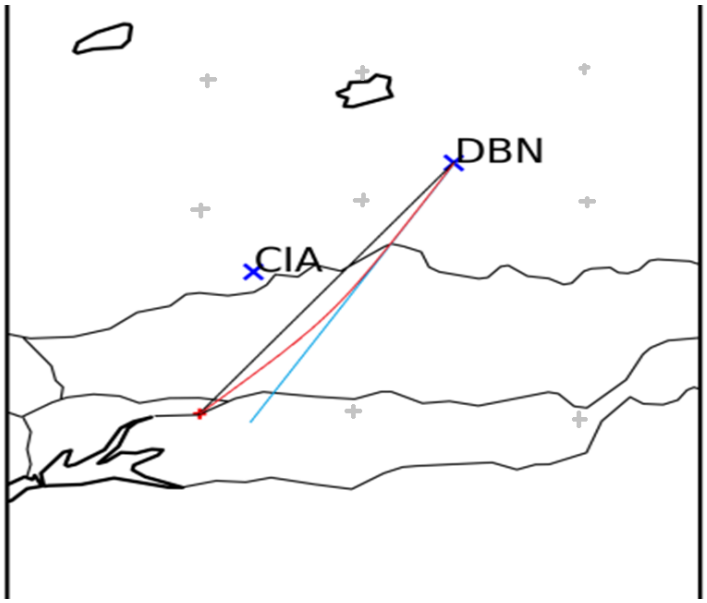

Figure 29: The nine discharge points are the red and grey '+'. The two infrasound detection stations are Cabauw (CIA) and De Bilt (DBN), indicated with a blue cross. The black line is the theoretical back-azimuth between discharge and detector. The blue line is the measured-back azimuth and the red line is the ray path. This is the path which the sound wave has travelled.

3.2.6 Investigation of detections around 09:25 UTC

As stated here above there was also a thunderstorm passing De Bilt around 9:25 UTC (34000 s), suggested by the infrasound system (figure 26. In the figures 30 and 31 the lighting detections from FLITS and KLDN are stated, for a time range from 9:20 UTC till 9:40 UTC. In a range of 80 kilometers around De Bilt. The blue points are detections around 9:20 UTC and the red points are detections around 9:40 UTC. We see over time the detections come closer to De Bilt. Around the time of 9:40 UTC it starts to hitting De Bilt. The infrasound signal shows that there is a possible thunderstorm that strucks De Bilt around 9:25 UTC. The FLITS and KLDN systems are detecting lightning discharge 20 to 30 kilometers away from De Bilt at that time. So we have now 2 systems that give at 9:25 the lightning strikes 25 to 30 kilometers away and a system that gives the lightning strikes over De Bilt. To look which is right, we look to the radar images in figure 32 and 33. Figure 32 gives the radar image of 9:15 UTC. The green dot is De Bilt and it is clear that the thunderstorm or squall line is still 20 to 30 kilometers away, which was suggested by the FLITS and KLDN system. In figure 33 we see the radar image of 9:40 UTC. Here the thunderstorm is over De Bilt. All 3 systems shows that. So the detections by the infrasound system at 9:25 is no lightning strikes. It is probably an other infrasound source. What kind of source is unknown.

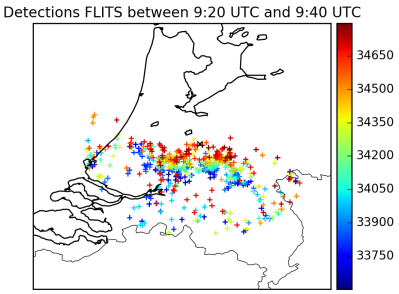

Figure 30: All lighting detections by the FLITS system between 9:20 and 9:40 UTC. With a distance of 80 km from De Bilt.

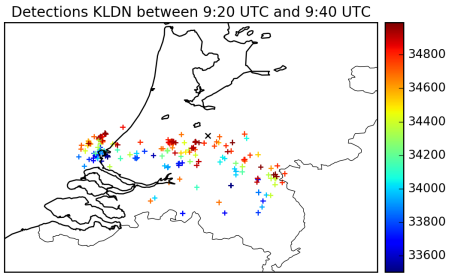

Figure 31: All lighting detections by the KLDN system between 9:20 and 9:40 UTC. With a distance of 80 km from De Bilt.

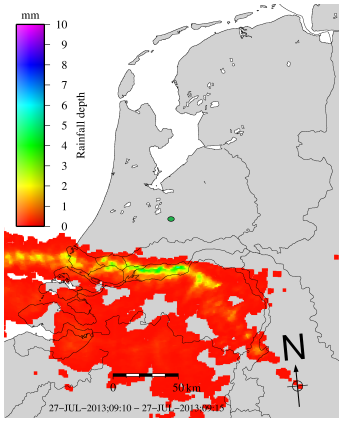

Figure 32: The radar image of 27-07-2013 9:10 - 9:15 UTC. The convergence line is where there is the green/yellow line. At this moment way south of De Bilt. On this line the lighting is the heaviest. The green dot is De Bilt.

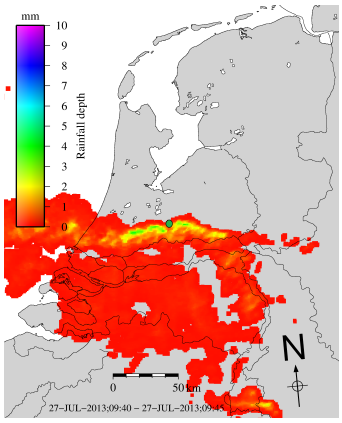

Figure 33: The radar image of 27-07-2013 9:40 - 9:45 UTC. The convergence line is where there is the green/yellow line. At this moment at De Bilt. On this line the lighting is the heaviest. The green dot is De Bilt.

3.2.7 The discharge of 9:48:29 UTC

With one discharge we will show the detection with the Fisher ratio, apparent velocity and back-azimuth. Furthermore, the discharge goes in the propagation program, so we can see how the rays will propagate through the atmosphere at that time. With that information we can couple the infrasound detections with the detections from KLDN and FLITS. This will only be done for the cloud-to-ground (CG) discharges.

The discharge which is investigated is the discharge at 9:48:29 UTC. 27 seconds earlier KLDN has also detected a discharge at an azimuth of 272°. The discharge was at 8.8 kilometers from De Bilt. In figure 34 we have in the upper panel the bestbeam outcome. in the second panel the Fisher ratio, in the third is the apparent velocity and in the last panel the back-azimuth. For this discharge we have an Fisher ratio of 73, an apparent velocity of 383 m/s and an back-azimuth of 263°.

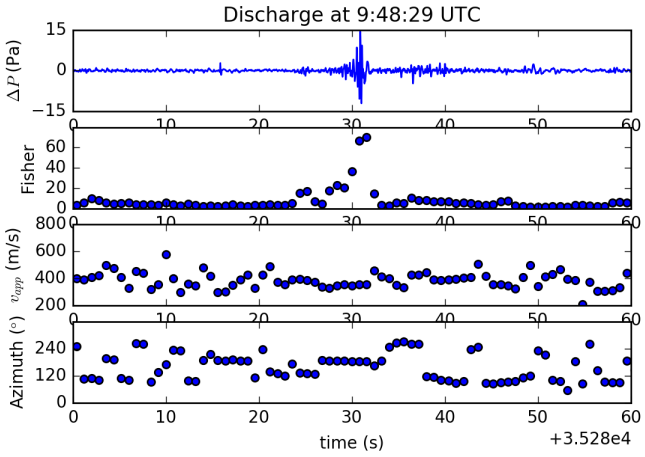

Figure 34: A close look to the discharge of 9:48:29 UTC. In the first frame there is the bestbeam output of the system. In the second frame we have the Fisher ratio. In the third the apparent velocity and in the last frame the back azimuth.

Now we have to look if these two separate detections are from 1 discharge. At first we look to the time delay. The time delay is 26.6 seconds. From figure 22 we see that the sound speed was at that time 0.346 km/s. So theoretical it takes 25.4 seconds from source to the detector here in De Bilt. The assumption here is that it travels over the surface in a horizontal plane. We have now a time difference between the theoretical time delay and the measured time delay of 1.6 seconds. This corresponds to a distance difference of 553 meter. This is just inside the error of the KLDN system, 600 meter.

Besides the time we can also look to the back-azimuth. The back-azimuth of the KLDN system is 272°, while the infrasound has a back-azimuth of 263°. This is an azimuth difference of 9°. This 9°error leads to a miss location by 1.4 kilometers, well outside the limits of the KLDN system. So in the first place we will say that this is not the same source in KLDN and the infrasound system. This is than no match between the

infrasound and KLDN system. Now the 3D propagation model comes in, which is seen in figure 35.

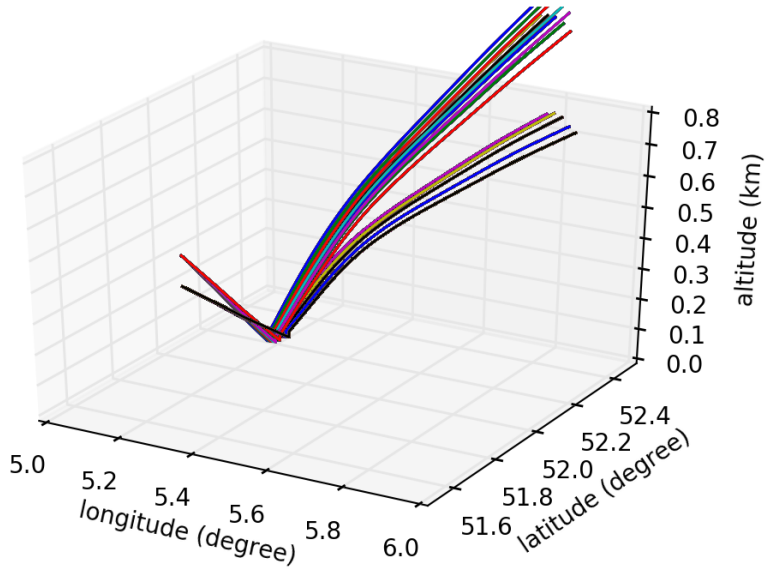

Figure 35: 3D ray tracing from the 3D ray equations. This is for the discharge at 9:48:28 UTC. The source of the sound is at 300m height and at 400m height.

In figure 35 we have shot the rays with a declination between 70°till 100°, at an 1°resolution. The inclination goes from 0°till 15°and from 280°till 360°with an resolution of 1°. We vary the altitude between 0 and 1000 meters. With a resolution of 100 meters. The rays that are shown in figure 35 have a bounce point at the coordinates (52.10°N,5.18°E). This are the coordinates of the infrasound array at De Bilt. The rays that are shown come from an altitude of 300 and 400 meters. Furthermore the rays have an azimuth wind-error of 6.1°for the 300 meter ray and 6.5°at the 400 meter ray. Now we count the 6.1°and 6.5°up to the measured back-azimuth of 263°, so we get an back-azimuth of 269.1°and 269.5°. Now the error location is for the 400 meter altitude ray 300 meters. For the 300 meter altitude ray is the error 360 meters.

3.2.8 Couple the KLDN and FLITS data with infrasound data

In the previous section there is shown how to couple a detection of the KLDN system with the infrasound system. Now we also take FLITS into account. To couple the detections of KLDN-infrasound, FLITS-infrasound and KLDN-FLITS, we only use cloud-to-ground discharges. At first the KLDN and FLITS system would couple. The coupling assumptions are following. The Δt is 1 second. This is due to that the internal clock of the systems could not be synchronised. Besides the time, there is also a uncertainty in the

location of the discharge. The largest uncertainty is by the FLITS network of 1.0 kilometer. This gives us a Δx of 1.4 kilometers. Now the coupling assumptions are known the systems could be coupled. The KLDN system has 80 CG detections and FLITS has 24 CG detections. When the systems are combined, the KLDN and FLITS systems have 8 similar CG discharges detected.

These 8 detections are now coupled to the infrasound dataset. So another coupling assumptions are needed. The assumption of Δx stays the same. The time assumption is now dependent of the distance of the discharge by the following equation:

$$\Delta t = \frac{\text{Distance}}{c_{eff}} \pm 3 \tag{23}$$

Because the infrasound dataset is coupled here, the azimuth shift has to take into account. Therefore the measured back-azimuth from the infrasound array is allowed to shift 10°from the back-azimuth of the electromagnetic system. Note that the infrasound array has an uncertainty 2-3°in the back-azimuth and about 20 m/s in the apparent veleocity. Now the assumptions are known the discharges could be coupled. There are 8 discharges from FLITS/KLDN and with these assumptions 2 out of 8 detections are coupled with the infrasound dataset.

Now we take the KLDN and FLITS system apart of each other and couple them separately to the infrasound system. At first the system FLITS is taken. The same coupling assumptions are taken as from the coupling of FLITS/KLDN/infrasound. From the 24 cloud-to-ground detections of FLITS, the infrasound array detected 5 cloud-to-ground discharges. FLITS has a lot of cloud-to-cloud detections, 1719 detections, it is possible that the FLITS system has miss characterized the discharges. So we do the coupling system again, but now for the cloud-to-cloud detections. These detections we will couple with the infrasound data. There are probably 80 of the 1719 detections miss matched. So they are characterized as a cloud-to-cloud discharge, but they are maybe a cloud-to-ground discharge. Further validation has to be done to be sure this is a miss characterisation of the system. This validation could be done by a second infrasound array in Cabauw. So cross-bearing could be done.

At last the KLDN system is coupled with the infrasound dataset. The assumptions are almost the same. Only the localisation uncertainty is in the KLDN system smaller : 0.6 km. This gives a Δx of 0.85 kilometers, or 850 meters. KLDN has 80 cloud-to-ground detections. 15 of the 80 detections are coupled with the infrasound dataset. As what there is done by FLITS there is also looked if KLDN has miss characterisation. KLDN has 318 cloud-to-cloud detections. 20 of these detections are probably detected by the infrasound array. So 20 of the 318 detections are probably miss matched. But like as the FLITS system further research has to be done to look if these are real miss characterisations or that it are other infrasound sources.

4 Conclusion & Discussion

In this study we looked to a way to validate the different lightning detections systems. This is done by putting the infrasound signal as reference. Before the validation could be started, the uncertainties of the propagation of the infrasound has to be known. From the propagation of infrasound we have the following results:

- The wind is a key player in the propagation of infrasound. A model that is used in this thesis shows the following result. In this case and windfield rays that propagate along the wind becomes a factor 1.5 further than rays that travel against the wind.
- The effective distance, the ratio between the effective sound speed at the ground and the maximum effective sound speed, is 25-30 kilometer. With the 1.5 factor that stated here above. The discharges which are along the wind are detected till maximum 50 kilometers. While discharges that are against the wind will detected till 20 kilometers.
- Due to the cross-winds along the rays in the atmosphere the measured back-azimuth will be shifted away from the theoretical back-azimuth. In this case, the largest azimuth shift which is measured is $\pm$ 7°. This number is always changing due to its wind field.
- The 3D propagation model shows us that the rays which are detected at the infrasound array, are direct arrivals from the source. So there will be no bounce between the discharge and the array.
- To use a 3D propagation model a NWP model is critical. The best choice is a high-resolution non-hydrostatic model. Due to the convective characteristic of this kind of models. At KNMI this is the HARMONIE model.
- With this setup it is possible to look in detail to the infrasound propagation of the individual discharges.
- The comparison between FLITS and infrasound gives that 5 of the 24 detections from FLITS are detected in both systems. With a probability 80 of 1719 detections miss matched.
- The comparison between KLDN and infrasound gives that 15 of the 80 detections from KLDN are detected in both systems. Furthermore 20 of 315 detections from KLDN could be a miss match from the system.

Future studies may focus on:

- More case studies so that the effective distance become a specified number, with uncertainty analysis. Besides of the effective distance, something more could be also said about the azimuth shift. If there is for example a maximum azimuth shift. Or a kind of equation with gives with a certain amount of cross-wind an azimuth shift.
- Crossbearing with the array in Cabauw (CIA). In this case it was not possible due to the very low hits at the CIA array. Furthermore, the distance between De Bilt and Cabauw is almost to large. Because the effective distance is almost the distance between Cabauw and De Bilt (22 kilometers). Due to this, crossbearing is only possible in a small area.
- There could be detections missed by FLITS or KLDN which the infrasound system has picked up. So in further research it is good to use a Lightning Mapping Array and compare this to the FLITS and KLDN system and also with the infrasound dataset.
- In this study there is only looked at the CC discharges. When a next study will be done CC discharges have to be considered. With the detections of CC discharges, there could be explained why the FLITS network detected so much CC discharges.
- Other array processing techniques that are appropriate for near-field sources to localize acoustic sources with an array.
- In this thesis there is only looked that several rays. When infrasound is created there will be a continuous wave. The source is also an approximation. Here it is approximated to point sources, while a lightning discharge is a line source. For next studies it could be useful to use a full 3D wave model. So that there is a line source with a continuous wave.
- Not every infrasound detection is a lightning discharge. It is important to look at different meteorological parameters and to the waveforms from the station. To be sure that the signal from the station is a lightning discharge.

Acknowledgements

My Msc project has come to an end and therefore, I would like to thank various people for their help with my Msc project. In the first place my KNMI supervisors Dr. Jelle Assink and Dr. Hidde Leijnse, with their advice, enthusiasm and guidance were essential for this project. The discussions helped me a lot throughout the project to make it to a good end. I also wish to acknowledge the help provided by Dr. Aarnout van Delden, my supervisor from IMAU.

In addition, I would like to thank my study mates and the room mates from the KNMI for the support. At last I would like to thank my lovely family and especially my parents and sister who supported me for 23 years to finally get here. And of course I wish to thank is my great love Tamar who supported me in a way I could only dream about it.

References

[1] Schade in beeld: Onweer en bliksem. https://www.nn.nl/OverNationaleNederlanden/Pers-1/Persbericht/Schade-in-beeld-Onweer-en-Bliksem.htm., 2014-12-01.

[2] Werkinstructies elektrische ontladingen op eham en ehrd. Werkinstructies weerkamer KNMI, 2016-08-22.

[3] L. de Vos. Intercomparison of the flits and kldn with atdnet lightning detection systems in the netherlands, with a case study on the potential of infrasound lightning detection. Master's thesis, University of Utrecht, 2015.

[4] I. Holleman, H. Beekhuis, S. Noteboom, L. Evers, H. Haak, H. Falcke, and L.Bähren. Infrasonic signals from thunder. *J. Geophys. Res.*, 84(C4), 1979.

[5] J.D. Assink, L.G. Evers, I. Holleman, and H. Paulssen. Characterization of infrasound from lightning. *Geophysical Research Letters*, 35(15), 2008.

[6] T. Farges and E. Blanc. Characteristics of infrasound from lightning and sprites near thunderstorm areas. *J. Geophys. Res.*, 115, 2010.

[7] D.R. Poelman. On the science of lightning: An overview. *Wetenschappelijke en Technische publicatie*, (56).

[8] A. Le Pichon, E. Blanc, and A. Hauchecorne. *Infrasound monitoring for atmospheric studies*. Springer, Dordrecht, 2010.

[9] L. G. Evers. *The inaudible symphony: on the detection and source identification of atmospheric infrasound*. PhD thesis, TU Delft, Delft University of Technology., November 2008.

[10] P. Campus. The ims infrasound network and its potential for detection of events: examples of a variety of signals recorded around the world. *Inframatics*, 6:14–22, 2004.

[11] P. Campus and D. Christie. *Worldwide observations of infrasonic waves. In Infrasound Monitoring for Atmospheric Studies*, pages 185–234. Springer, Dordrecht, 2010.

[12] A.J. Dessler. Infrasonic thunder. *J. Geophys. Res.*, 78(12):1889–1896, 1973.

[13] A.A. Few. *The Earth's Electrical Environment*, chapter Acoustic radiations from lightning, pages 46–60. Natl. Acad., Washington, D.C., 1986.

[14] I. Holleman. *Handboek Waarnemingen*, chapter Hoofdstuk 20, Bliksem. KNMI, 2005.

[15] A.A. Few. Power spectrum of thunder. *J. Geophys. Res.*, 74(28):6926–6934, 1969.

[16] C.R. Holmes, M. Brook, P. Krehbiel, and R. McCrory. Reply on "on the power spectrum and mechanism of thunder. *J. Geophys. Res.*, 76(30):7443, 1971.

[17] C.R. Holmes, M. Brook, P. Krehbiel, and R. McCrory. On the power spectrum and mechanism of thunder. *J. Geophys. Res.*, 76(30):2106–2115, 1971.

[18] N.K. Balachandran. Validation of an operational lightning detection system. *ILDC / ILMC Validation of Operational LDS*, 2006.

[19] A.A. Few. Lightning channel reconstruction from thunder measurements. *J. Geophys. Res.*, 75:7517–7523, 1970.

[20] A.A. Few and T.L. Teer. The accuracy of acoustic reconstructions of lightning channels. *J. Geophys. Res.*, 79:5007–5011, 1974.

[21] D.R. MacGorman, A.A. Few, and T.L. Teer. Layerd lightning acitivity. *J. Geophys. Res.*, 86:9900–9910, 1981.

[22] L-J. Gallin, T. Farges, R. Marchiano, F. Coulouvrat, and E. Defer. Statistical analysis of storm electrical discharges reconstituted from a lightning mapping system, a lightning location system, and an acoustic array. *J. Geophys. Res. Atmos.*, 121, 2016.

[23] J.D. Assink. The inaudible sound of thunderstorms. Master's thesis, University of Utrecht, 2007.

[24] R. Boonstra. Validation of safir/flits lightning detection system with railway-damage reports. Technical report, KNMI, 2008.

[25] C. Druë, T. Hauf, U. Finke, S. Keyn, and O. Kreyer. Comparison of a safir lightning detection network in northern germany to the operational blids network. *J. Geophys. Res. Atmos.*, 112:1984–2012, 2007.

[26] D.R. Poelman, W. Schulz, and C. Vergeiner. Performance characteristics of distinct lightning detection networks covering belguim. *Journal of Atmospheric and Oceanic Technology*, 30(5):942–951, 2013.

[27] D.R. Poelman, F. Honoré, G. Anderson, and S. Pedeboy. Comparing a regional, subcontinental, and long-range lightning location system over the benelux and france. *Journal of Atmospheric and Oceanic Technology*, 30(10):2394–2405, 2013.

[28] O.A. Godin. An effective quiescent medium for sound propagating through an inhomogeneous, moving fluid. *J. Acoust. Soc, Am.*, pages 1269–1275, 2002.

[29] P.S.M. Smets, J.D. Assink, A. Le Pichon, and L.G. Evers. Ecmwf ssw forecast evaluation using infrasound. *J. Geophys. Res. Atmos.*, 121(9):4637–4650, 2016.

[30] R.A. Fisher. *Statisctical methods for research workers.* Oliver and Boyd, London, 1948.

[31] B.S. Melton and L.F. Bailey. Multiple signal correlators. *Geophysics*, pages 565 – 588, 1957.

[32] J.V. Olsen. Infrasound signal detection using the fisher f-statistic. *Inframatics*, 2004.

[33] M.R. Spiegel and L.J. Stephens. *Statistics.* McGraw-Hill, 2008.

[34] J.D. Assink. *Infrasound as upper atmospheric monitor*. PhD thesis, The University of Mississippi, University, MS, USA, 2012.

[35] J.F. Lingevitch, M.D. Collins, and W.L. Siegmann. Parabolic equation for gravity and acousto-gravity waves. *J. Acoust. Soc, Am.*, 105:3049–3056, 1999.

[36] E. Andersson. *User guide to ECMWF forecast products*. ECMWF, 2015.

[37] C. Azorin-Molina, S. Tijm, E.E. Ebert, S.M. Vicente-Serrano, and M.J. Estrela. Sea breeze thunderstorms in the eastern iberian peninsula. neighborhood verification of hirlam and harmonie precipitation forecasts. *Atmospheric Research*, 139(2014):101–115, 2014.

[38] P. Blom and R. Waxler. Impulse propagation in the nocturnal boundary layer: Analysis of the geometric component. *The Journal of the Acoustical society of America*, 131(5), 2012.

[39] F.B. Jensen, W.A. Kuperman, M.B. Portor, and H. Schmidt. *Computational Ocean Acoustics*. Springer, 2000.

[40] L.C. Sutherland and H.E. Bass. Atmospheric absorption in the atmosphere up to 160 km. *J. Acoust. Soc. Am.*, 115(3):1012–1032, 2004.

[41] H.E. Bass and C.H. Hetzer. An overview of absorption and dispersion of infrasound in the upper atmosphere. *Inframatics*, (15), 2006.

[42] S.A. Briels. Infrasound source location. Master's thesis, Delft University of Technology, 2010.